© 2015. Published by The Company of Biologists Ltd | Development (2015) 142, 2951-2961 doi:10.1242/dev.123174

RESEARCH ARTICLE

Single-cell analysis of endothelial morphogenesis *in vivo*

Jianxin A. Yu, Daniel Castranova, Van N. Pham and Brant M. Weinstein*

ABSTRACT

Vessel formation has been extensively studied at the tissue level, but the difficulty in imaging the endothelium with cellular resolution has hampered study of the morphogenesis and behavior of endothelial cells (ECs) *in vivo*. We are using endothelial-specific transgenes and high-resolution imaging to examine single ECs in zebrafish. By generating mosaics with transgenes that simultaneously mark endothelial nuclei and membranes we are able to definitively identify and study the morphology and behavior of individual ECs during vessel sprouting and lumen formation. Using these methods, we show that developing trunk vessels are composed of ECs of varying morphology, and that single-cell analysis can be used to quantitate alterations in morphology and dynamics in ECs that are defective in proper guidance and patterning. Finally, we use single-cell analysis of intersegmental vessels undergoing lumen formation to demonstrate the coexistence of seamless transcellular lumens and single or multicellular enclosed lumens with autocellular or intercellular junctions, suggesting that heterogeneous mechanisms contribute to vascular lumen formation *in vivo*. The tools that we have developed for single EC analysis should facilitate further rigorous qualitative and quantitative analysis of EC morphology and behavior *in vivo*.

KEY WORDS: Endothelial morphogenesis, Single-cell analysis, Plexin D1, Morphodynamics, Lumenization, Tight junction, Claudin 5

INTRODUCTION

The proper formation of functional blood vessel networks is essential for vertebrate organogenesis and physiological homeostasis (Chung and Ferrara, 2011). Insufficient or abnormal vessel growth frequently results in organ malfunction and is associated with diseases such as tumor growth and age-related macular degeneration (AMD) (Chung and Ferrara, 2011). During angiogenesis, new vessels assemble from vascular sprouts emerging from previously formed parental blood vessels. Once neighboring sprouts interconnect, in a process called anastomosis, newly formed vessel segments stabilize, lumenize, and form a functional network with directional blood circulation. At the sub-tissue level, different regions of sprouting vessels exhibit unique characteristics, including heterogeneous phenotypes and distinct gene expression signatures (Aird, 2012). Endothelial cell (EC) populations are not homogenous in different vascular beds or between normal physiological and pathological conditions (Aird, 2007a,b; Nolan et al., 2013). Characterization of ECs in different regions of sprouting vessels demonstrates that vascular morphogenesis is a dynamic process with the spatial and temporal differentiation of a variety of coordinated cell behaviors, including directional polarization, collective migration, cell division and lumen formation (Wacker and Gerhardt, 2011). During sprouting, a leading 'tip cell' directs migration, while 'stalk cells' behind undergo nascent lumen formation. Although these are not defined differential EC fates [tip and stalk cells can and do frequently interchange (Jakobsson et al., 2010; Pelton et al., 2014)], tip and stalk cells have been shown to display differential gene expression and distinct morphological features (del Toro et al., 2010; Gerhardt et al., 2003; Strasser et al., 2010).

Most of the available data on vascular morphology and dynamics are from *in vitro* and *ex vivo* experimental models. Technical challenges in high-resolution optical imaging of deep tissues and lack of suitable genetic tools for imaging ECs at single-cell resolution have hampered study of the cell biology of ECs *in vivo*. This is certainly true for the process of vascular tubulogenesis, a multistep interwoven developmental process involving initiation, expansion and stabilization of the nascent lumen. Recent reports have highlighted a number of different mechanisms potentially involved in the assembly of vascular tubes (Charpentier and Conlon, 2014). Cord hollowing with cellular rearrangements or cell hollowing involving fusion of intracellular vacuoles have both been proposed as mechanisms for lumen formation based on observations from *in vitro* cell culture, tissue sections, and live imaging of animal models (Folkman and Haudenschild, 1980b; Iruela-Arispe and Beitel, 2013; Lubarsky and Krasnow, 2003). Adhesion to surrounding extracellular matrix (ECM), loss of some EC-EC contacts, or repulsive interaction between EC surfaces have all been suggested as important forces promoting expansion of nascent lumenal spaces (Eilken and Adams, 2010; Lampugnani et al., 2010; Strilic et al., 2010, 2009; Wang et al., 2010; Zovein et al., 2010). Other work, primarily *in vitro*, has uncovered molecular regulators crucial for lumenogenesis (Bayless and Davis, 2002; Bayless et al., 2000; Egginton and Gerritsen, 2003; Iruela-Arispe and Davis, 2009; Koh et al., 2009, 2008; Popson et al., 2014; Sacharidou et al., 2010, 2012).

The zebrafish has recently emerged as an important model organism for studying the growth and morphogenesis of blood vessels during development (Butler et al., 2011; Gore et al., 2012; Isogai et al., 2003; Kamei et al., 2006; Zovein et al., 2010). A variety of recent studies have taken advantage of the optical clarity of zebrafish embryos and larvae to carry out live imaging of tubulogenesis in developing vessels within living animals (Ellertsdottir et al., 2010; Herbert and Stainier, 2011; Herwig et al., 2011; Jin et al., 2005, 2007; Kalen et al., 2009; Kamei et al., 2006; Lenard et al., 2013; Wang et al., 2010). These studies have provided *in vivo* evidence substantiating both the cell hollowing and the cord hollowing models for lumenogenesis. However, difficulties in distinguishing closely apposed ECs using available transgenic tools have made it difficult to comprehensively and accurately assess the contributions of individual ECs to lumen assembly and morphogenesis of vessels in general. In order to monitor the morphology and dynamic behaviors of individual ECs, we have

Program in Genomics of Differentiation, The Eunice Kennedy Shriver National Institute of Child Health and Human Development, National Institutes of Health, Bethesda, MD 20892, USA.

*Author for correspondence (weinsteb@mail.nih.gov)

Received 11 February 2015; Accepted 27 July 2015

Development (2015) 142, 2951-2961 doi:10.1242/dev.123174

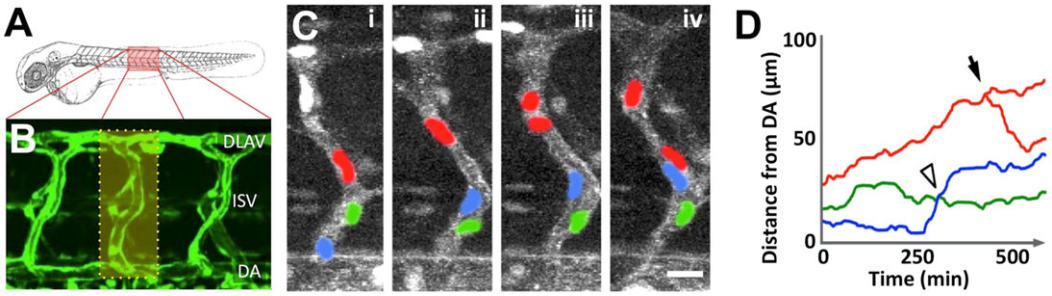

Fig. 1. Complex cellular architecture and behavior of ECs in the developing zebrafish trunk. (A) Schematic of a zebrafish embryo illustrating the position of trunk vessels imaged in B. (B) Confocal image of trunk ISVs and DLAVs in a 48 hpf *Tg(fli1a:egfp)*^{y1} embryo. (C) Confocal image time series of a single growing trunk ISV sprout in a *Tg(fli1a:nls-egfp)*^{y7}*; Tg(kdrl:mcherry-caax)*^{y171} double-transgenic embryo at 31 (i), 34 (ii), 37 (iii) and 40 (iv) hpf. The mCherry-positive ECs are in gray, while eGFP-positive EC nuclei are highlighted in red, blue and green. (D) Quantitative measurement of the dorsal-ventral position [distance from the dorsal aorta] of each of the endothelial nuclei in C, measured every 10 min over a 10 h timecourse. The arrowhead shows where two EC nuclei exchanged positions in the vessel segment and the arrow shows where a nuclear division occurred. DA, dorsal aorta; DLAV, dorsal longitudinal anastomotic vessel; ISV, intersegmental vessel. Scale bar: 20 µm.

developed new transgenic tools that simultaneously label both the nuclei and the plasma membranes or tight junctions of single ECs with different fluorescent proteins. Using high-speed confocal and two-photon imaging of these transgenes in injected mosaics, we are able to identify individual ECs and image and parse some of the complex cellular and subcellular dynamics of individual cells that contribute to vessel sprouting and lumen formation.

RESULTS

Dynamic and complex collective cell behaviors during trunk angiogenesis

The trunk intersegmental vessels (ISVs) of the developing zebrafish provide a valuable model for investigating sprouting angiogenesis (Isogai et al., 2003; Lawson and Weinstein, 2002). The relatively simple cell composition, repeating pattern and stereotypical assembly (supplementary material Fig. S1) of these vessels make them ideal for examining *in vivo* cellular behaviors during sprouting angiogenesis and lumenization (Fig. 1A,B). However, available transgenic tools do not permit reliable identification of single ECs and tracking and imaging of their morphology and behavior, making it difficult to assess how individual ECs contribute to the assembly of the functional vessels. ECs migrate collectively and are extensively intertwined with one another in vascular sprouts. They also display highly dynamic behaviors in growing vessel segments.

We used two-photon time-lapse imaging to examine the movements of entire populations of ECs in developing ISVs in *Tg(fli1a:nls-egfp)*^{y7}*; Tg(kdrl:mcherry-caax)*^{y171} double-transgenic animals with green fluorescent EC nuclei and red fluorescent EC membranes (Fig. 1C,D). ECs in growing ISVs are highly dynamic, undergoing cell division, passing one another, and exchanging positions within extending vascular sprouts (Fig. 1C,D; supplementary material Movie 1). As visualized in the *Tg(fli1a:egfp-F)*^{y288} transgenic line, ISV sprouts also extend numerous protrusions that appear and disappear, and the overall morphology of the extending ISV sprouts can change dramatically from one time point to the next (supplementary material Fig. S2A). Using these and other available transgenic lines it is not possible to accurately distinguish boundaries between ECs in growing vessel segments, or to assess the morphology and dynamics of individual ECs. By creating mosaics by injecting *Tg(fli1a:egfp-F)*^{y288} endothelial expression constructs into *Tg(kdrl:mcherry-caax)*^{y171} germline transgenic zebrafish, it is possible to image subportions of the developing vasculature in isolation (supplementary material Fig. S2B, arrows). However, it is impossible to determine with certainty whether these represent individual ECs or multiple adjacent cells. In order to parse complicated, interwoven EC behaviors we designed a novel transgenic approach to identify and analyze the morphology of individual ECs.

Visualizing individual ECs within developing zebrafish embryos

To investigate the detailed architecture and dynamic behaviors of individual cells within developing blood vessels, we developed transgene constructs to reliably mark single ECs. We prepared Tol2 transgene constructs in which the *fli1a* endothelial promoter (Lawson and Weinstein, 2002) drives expression of H2B-TagBFP (nuclear-localized blue fluorescence) followed by eGFP-farnesyl (membrane-localized green fluorescence), linked together by the self-cleaving p2A peptide (Kim et al., 2011) permitting stoichiometric co-translation of both fluorescent proteins (Fig. 2A). This *Tol2(fli1a:h2b-tagBFP-2A-egfp-f)* transgene is used to generate mosaics by injecting it into *Tg(kdrl:mRFP-F)*^{y286} germline transgenic animals, allowing simultaneous observation of the nucleus (blue fluorescence) and membranes (green fluorescence) of the same EC and, therefore, conclusive determination of the number of ECs being observed and the identification of single cells, all in the context of the complete vasculature (red fluorescence) (Fig. 2B).

ECs expressing the injected transgene (blue/green/red) do not show any evidence of growth delay or altered morphology or behavior compared with adjacent non-transgene-expressing ECs (red only), and injected animals are otherwise indistinguishable from their uninjected siblings (data not shown). The membrane-tethered eGFP-farnesyl protein permits clear identification of cell membranes and fine membrane-based subcellular structures, such as intracellular vesicles and extending processes (Fig. 2B). Thus, this approach allows us to investigate the morphology and dynamic behaviors of single ECs during vascular development in the living animal.

EC morphology in the developing embryonic trunk vascular network

We used single-cell analysis to examine the morphology of ECs contributing to ISVs during their initial assembly in the zebrafish trunk. The trunk vessel network forms in a stereotypic fashion (Isogai et al., 2003). Angiogenic sprouts emerge from the dorsal aorta, extending dorsally along the intersomitic boundaries until they reach the dorsal-lateral surface of the neural tube

Development (2015) 142, 2951-2961 doi:10.1242/dev.123174

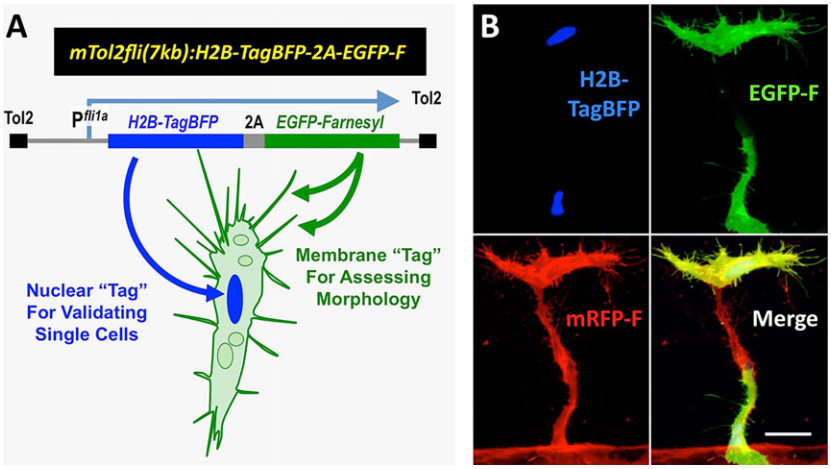

Fig. 2. Design and validation of an expression cassette for analyzing the morphology and dynamics of individual ECs within developing vessels. (A) The *Tol2(fli1a:H2B-TagBFP-p2A-egfp-F)* transgene construct for simultaneously marking endothelial nuclei (with H2B-TagBFP) and EC internal and plasma membranes (with eGFP-farnesyl). (B) Confocal micrograph of a growing trunk ISV/DLAV segment in a 32 hpf *Tg(kdrl:mRFP-F)*^{y286} embryo injected with a *Tol2(fli1a:H2B-TagBFP-p2A-egfp-F)* transgene, showing blue, green and red fluorescent channels and all three merged. This segment contains two individual transgene-labeled ECs (as indicated by the presence of a single H2B-TagBFP nucleus in each). eGFP-F fluorescence is concentrated on the cell surface as well as on internal membranes, although not readily evident in this low-magnification reconstructed image. Scale bar: 20 µm.

(supplementary material Fig. S1) (Isogai et al., 2003). Here, they branch rostrally and caudally and fuse with similar vascular sprouts from adjacent ISV segments to form continuous dorsal longitudinal anastomotic vessels (DLAVs).

We generated mosaics containing identifiable single ECs by injecting the *Tol2(fli1a:h2b-tagBFP-2A-egfp-f)* transgene into *Tg(kdrl:mRFP-F)*^{y286} germline transgenic animals as noted above. By examining a large number of individual ECs within the ISV at stages just post-DLAV interconnection, as assembly of the ISV/DLAV network is completed and lumenization is beginning, we are able to identify a number of different morphological classes (Fig. 3). Half of the ECs are found exclusively within the dorsally extending ISV segments, with a limited number extending the entire length of the ISV (Class I, 4.9%; Fig. 3A) but most extending only part way along the ISV (Class II, 45.1%; Fig. 3B). Other cells are found exclusively within the DLAV (Class III, 11.7%; Fig. 3C) or in an 'L' shape bridging the DLAV and ISV (Class IV, 16.7%; Fig. 3D) or bridging the ISV and dorsal aorta (Class V, 21.6%; Fig. 3E). The five classes and their relative proportions are summarized in Fig. 3F,G.

Higher magnification imaging of ECs within newly formed ISVs shows that they are often extensively interdigitated with one another, frequently extending fine processes along the vessel well beyond where the nucleus and main body of the cell are situated (Fig. 3H,I). This shows that cell-cell contacts between ECs in the trunk vascular network are complex, making it difficult to accurately discern EC boundaries and morphology without methods that reliably permit the identification and visualization of single ECs.

Measurement of protrusive activity and polarity in single ECs *in vivo*

Vessel sprouting involves the collective migration of a cohesive group of asymmetrically polarized ECs, with more and longer protrusions at their leading ends and fewer and shorter protrusions at their trailing ends. Although a recent study reported that partial inhibition of actin polymerization and EC protrusion does not limit ISV growth (Phng et al., 2013), the correlation between protrusive activity and directional migration of ECs *in vivo* remains largely unexplored and difficult to measure quantitatively. We used our single-cell imaging tools to investigate spatial and temporal morphodynamics of endothelial tip and stalk cell protrusions in growing ISVs of either normal animals or those defective in trunk ISV guidance and assembly due to loss of *plexin D1* (*plxnd1*).

In a previous study, we showed that growing ISV sprouts in zebrafish lacking the endothelial-specific semaphorin receptor Plxnd1 are unable to respond to somite-derived semaphorin guidance cues that normally restrict their growth to intersomitic boundaries, resulting in loss of proper directionality in their growth and the formation of disorganized trunk ISV networks (Torres-Vazquez et al., 2004) (Fig. 4A-D). Since *plxnd1* morpholino-injected animals exhibit identical phenotypes to *plxnd1*^{fov01b} mutants, without additional off-target effects (Torres-Vazquez et al., 2004), we used morpholino knockdown to examine and quantitate the morphology and dynamics of verified individual *plxnd1*-deficient *Tol2(fli1a:h2b-tagBFP-2A-egfp-f)* ECs in *Tg(kdrl:mRFP-F)*^{y286} germline transgenic animals (Fig. 4E,F). Visual inspection suggested that ECs indeed display loss of directional growth, but to determine whether this could be validated using objective metrics and to gain insights into the relationship between endothelial protrusiveness and loss of directionality, we performed a rigorous quantitative analysis of single EC protrusions. For each of six individual randomly chosen trunk ECs found above the level of the dorsal aorta, we measured the length of all of their protrusions (filopodia). The average total length of endothelial protrusions was similar between control and *plxnd1* morphant animals (Fig. 4G). To examine the directionality of these protrusions, we grouped the direction of measured protrusions into three categories depending on whether the filopodia were oriented in a dorsal (120° arc), lateral (60° arcs, 'side') or ventral (120° arc) direction (Fig. 4H). We measured protrusions in tip cells and stalk cells separately in both control and *plxnd1* morphants (Fig. 4I,J). There was a small but statistically significant increase in side and ventral protrusiveness along with a less significant decrease in dorsal protrusiveness in the tip cells of *plxnd1* morphants compared with controls (Fig. 4I). For stalk cells, *plxnd1* morphants showed more substantial increases in protrusiveness compared with controls, particularly dorsal and ventral protrusions (Fig. 4J). The lack of change in average protrusion length (Fig. 4G) and changes in the distribution of protrusions (Fig. 4I,J) together suggest that the spatial distribution and not total amount of protrusiveness is altered in *plxnd1*-deficient endothelial tip cells. The more pronounced effect on stalk cells compared with tip cells also hints that reduced EC-EC contact inhibition could be a contributing factor to the increased sprouting and branching of trunk vessels observed in the *plxnd1*-deficient animals.

Endothelial membrane protrusions are not static structures, but transient membranous extensions with highly dynamic behaviors. We used time-lapse two-photon imaging of *Tol2(fli1a:h2b-*

Development (2015) 142, 2951-2961 doi:10.1242/dev.123174

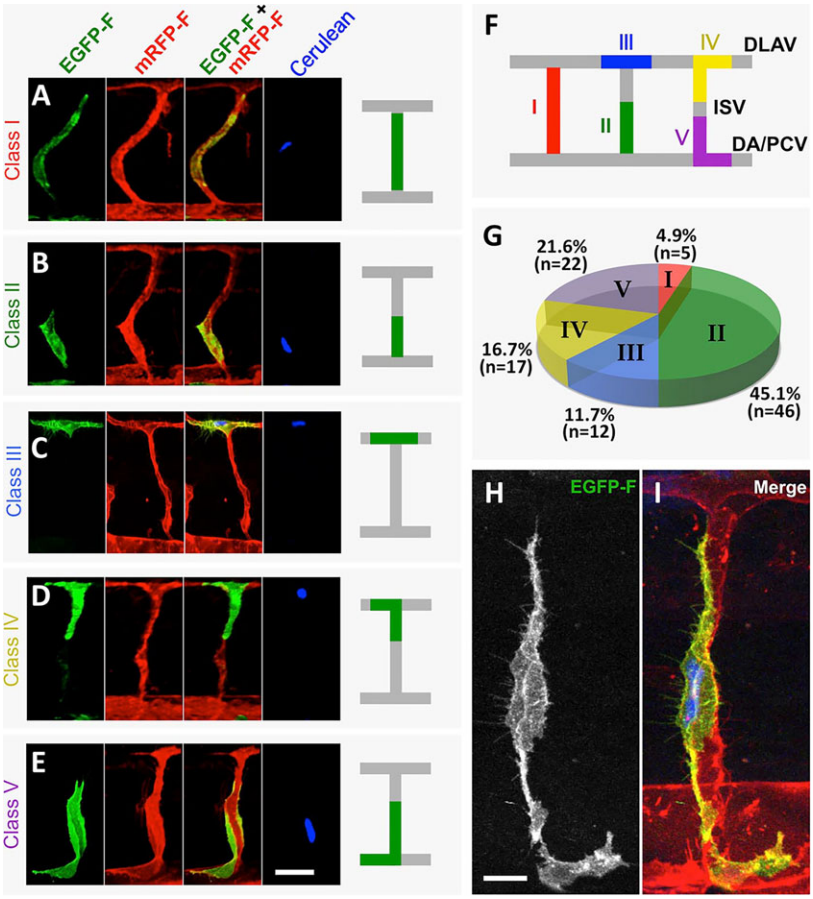

Fig. 3. Heterogeneous morphology of individual ECs in newly forming ISV/DLAV segments. (A-E) Representative confocal micrographs of verified single *Tol2(fli1a:H2B-TagBFP-p2A-egfp-F)* transgene-expressing ECs in trunk ISV/DLAV segments in a 42 hpf *Tg(kdrl:mRFP-F)*^{y286} germline transgenic embryo, showing green, red, red/green merge and blue fluorescent channels. (F) Morphological classification of ECs contributing to the ISV/DLAV. Class I, extending along an entire ascending ISV segment (see A); Class II, extending partially along an entire ascending ISV (see B); Class III, exclusively in the DLAV (see C); Class IV, in both DLAV and ISV (see D); Class V, in both DA and ISV (see E). (G) Quantification of the proportion of ECs found in each of the five morphological classes. (H,I) High-magnification GFP fluorescence (H) and merged GFP/BFP/RFP fluorescence (I) images of a representative verified single *Tol2(fli1a:H2B-TagBFP-p2A-egfp-F)* transgene-expressing EC in a trunk ISV segment in a 42 hpf *Tg(kdrl:mRFP-F)*^{y286} germline transgenic embryo, showing the morphological complexity of the cell, with fine processes extending up and down the vessel segment past the main part of the EC body. PCV, posterior cardinal vein. Scale bars: 20 µm in A-E; 10 µm in H,I.

tagBFP-2A-egfp-f)-injected *Tg(kdrl:mRFP-F)*^{y286} animals to capture and evaluate the temporal dynamics of filopodia in single *plxnd1*-deficient or control trunk ECs (Fig. 4K,L). Time-lapse recording revealed that membrane protrusions have a significantly longer average lifetime in *plxnd1*-deficient than in control ECs (Fig. 4M,N). Longer protrusive lifetimes were observed in both tip (Fig. 4M) and stalk (Fig. 4N) cells.

Single EC analysis reveals coexistence of both seamless transcellular lumens and multicellular sealed lumens in newly formed ISVs

As noted in the introduction, recent studies have suggested a number of possible mechanisms contributing to vascular lumen formation (Charpentier and Conlon, 2014). Lumen formation is thought to occur mainly by either cell hollowing (the formation of intracellular lumenal spaces by fusion of intracellular vacuoles) or cord hollowing (the generation of intercellular lumenal spaces by the rearrangement and creation of spaces between multiple ECs), although the extent to which lumen formation initiates intracellularly versus between cells is still not clear. As noted above, transgenic and other tools used to date for analysis of lumen formation *in vivo* have not permitted conclusive determination of how many cells are being examined, and therefore of where one cell ends and another cell begins, complicating interpretation.

As a first attempt to address these limitations, we began by using our single-cell analysis methods to determine the proportion of ECs in ISVs immediately after initial lumenization that contain enclosed lumens (i.e. lumenal spaces completely surrounded by a single EC). We captured images of single *Tol2(fli1a:h2b-tagBFP-2A-egfp-f)* ECs in *Tg(kdrl:mRFP-F)*^{y286} germline transgenic animals and then carried out 3D image reconstruction using active contour-based image segmentation to examine the cross-sectional profiles of the vessels that the ECs were incorporated in, to determine what proportion of each identified single EC was entirely enclosing the lumen (Fig. 5A). Frequently, cross-sectional profiles of identified single ECs revealed that the lumenal spaces adjacent to the ‘ends’ of the cell were surrounded by multiple cells (Fig. 5B; see cross-sections 1 and 4), as might be expected given the extensive interdigitation of ECs in assembling trunk vascular networks noted earlier, whereas the lumen adjacent to the middle of an EC was entirely enclosed by that single cell (Fig. 5B; see cross-sections 2 and 3). Lumen-enclosing ECs are detected in all positions in the ISV (Fig. 5C,D). Approximately one-third of all ISV/DLAV ECs are lumen enclosing (Fig. 5D, ‘Sum’), with substantially more lumen-enclosing ECs in the DLAV (Fig. 5D, Classes III and IV) and fewer in the more ventral ISV segments (Fig. 5D, Classes II and V). Of the lumen-enclosing cells, on average one-third of the length of each of these cells completely encircles the lumen at the time of initial lumenization (supplementary material Fig. S3), with additional cells abutting the lumen at the ends (see cross-sections 1 and 4 in Fig. 5B).

These observations suggest the coexistence of both unicellular and multicellular lumens in newly formed trunk ISVs. However, as discussed further below, the presence of unicellular lumens does not necessarily imply that these form ‘seamlessly’.

Analysis of endothelial junctions reveals coexistence of seamless, autocellular and multicellular sealed lumens

Intracellular lumen formation would be expected to not only result in unicellular lumenal spaces, but also to form them transcellularly

Development (2015) 142, 2951-2961 doi:10.1242/dev.123174

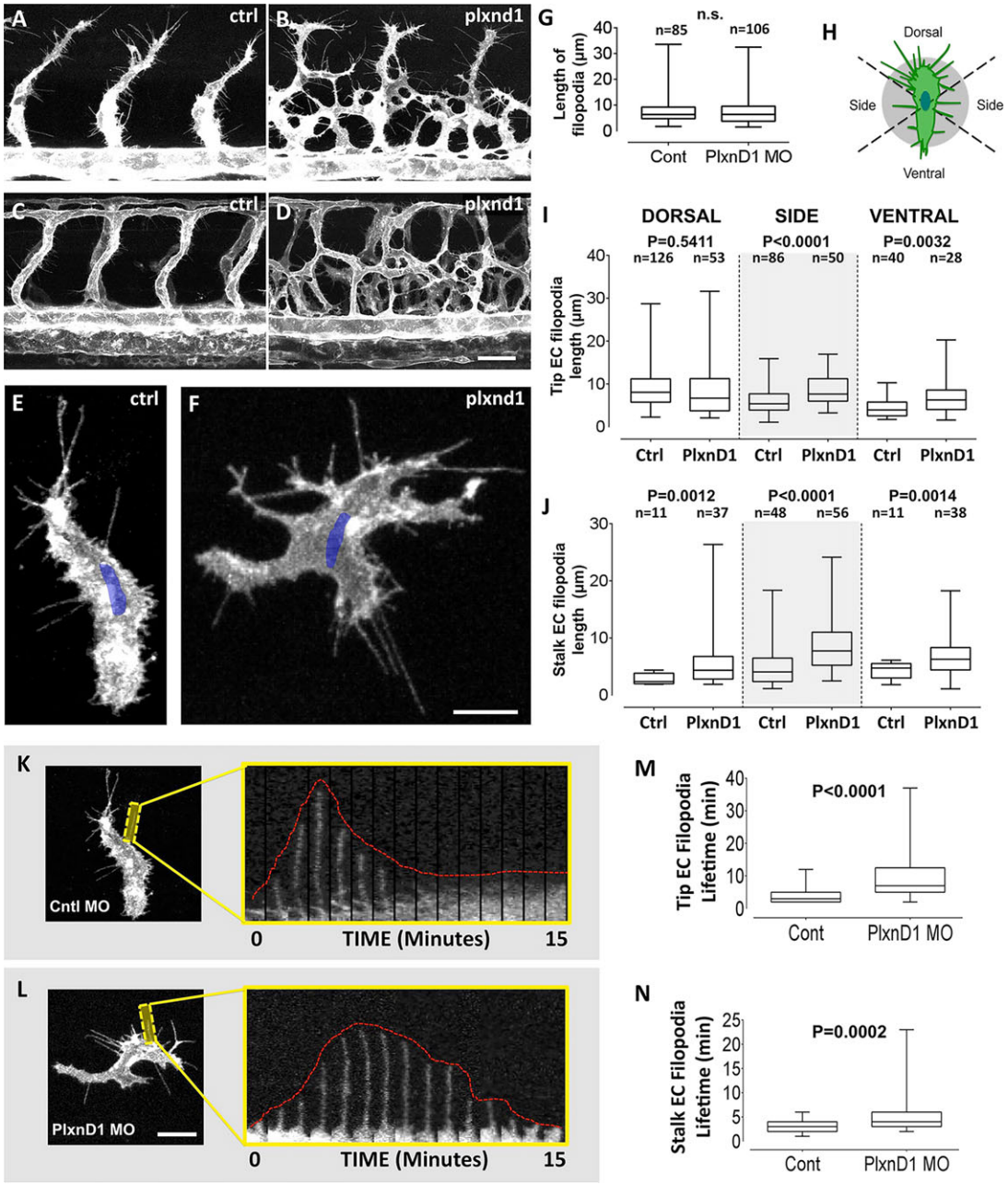

Fig. 4. Measuring endothelial protrusiveness, polarity and dynamics using single-EC imaging *in vivo*. The spatial distribution of filopodia in individual ECs is polarized during normal ISV network patterning. (A-D) Confocal images of mid-trunk vessels in 30 (A,B) or 42 (C,D) hpf in *Tg(fli1a:egfp)*^{y1} control (A,C) or *plxnd1* (B,D) morpholino-injected embryos, showing disorganization of the ISV network in Plxnd1-deficient animals. (E,F) Higher magnification confocal micrographs of verified single *Tol2(fli1a:H2B-TagBFP-p2A-egfp-F)* transgene-expressing ECs in the trunks of ∼30 hpf *Tg(kdrl:mRFP-F)*^{y286} control (E) or *plxnd1* (F) morpholino-injected embryos. GFP-F fluorescence is in gray, H2B-TagBFP-positive nuclei are in blue. (G) Quantification of the average total length of EC protrusions in ECs from control or *plxnd1* morpholino-injected embryos. (H) Diagram showing the quadrants used for assessing the directionality of endothelial protrusions – dorsal, ventral and side. (I,J) Quantification of the average total length of protrusions from (I) endothelial tip cells (cells at the leading front) and (J) endothelial stalk cells (cells not at the leading front) in control or *plxnd1* morpholino-injected embryos grouped by whether they protrude dorsally, to the side or ventrally. The data in G, I and J are collected from six independent experiments. (K,L) Representative confocal kymographs of endothelial protrusions on verified single *Tol2(fli1a:H2B-TagBFP-p2A-egfp-F)* transgene-expressing ECs in the trunks of ∼30 hpf *Tg(kdrl:mRFP-F)*^{y286} control (K) or *plxnd1* (L) morpholino-injected embryos. GFP-F fluorescence is in gray, H2B-TagBFP-positive nuclei are in blue. (M,N) Quantification of the average lifetime of protrusions emerging from (M) six endothelial tip cells (cells at the leading front) and (N) six endothelial stalk cells (cells not at the leading front) in control or *plxnd1* morpholino-injected embryos. The data in M and N were collected from four independent experiments. Box-and-whisker plots (G,I,J,M,N) represent interquartile range (spanning from first to third quartile with median segment inside) in the box, minimum and maximum values (whiskers) at both ends. *P*-values were derived by unpaired two-tailed Student's *t*-test. n.s., not significant. All images are lateral views with rostral to the left. Scale bars: 25 µm in A-D; 10 µm in E,F,K,L.

or 'seamlessly' without an autocellular junction (Fig. 6Ai). Autocellular junctions could result from lumen formation by single ECs 'wrapping' on themselves (Fig. 6Aii). The membrane-tethered fluorescent proteins used in the transgenes described thus far (*egfp-f*, *mRFP-F*) outline boundaries between cells but do not permit direct conclusive visualization of cell-cell or autocellular

Development (2015) 142, 2951-2961 doi:10.1242/dev.123174

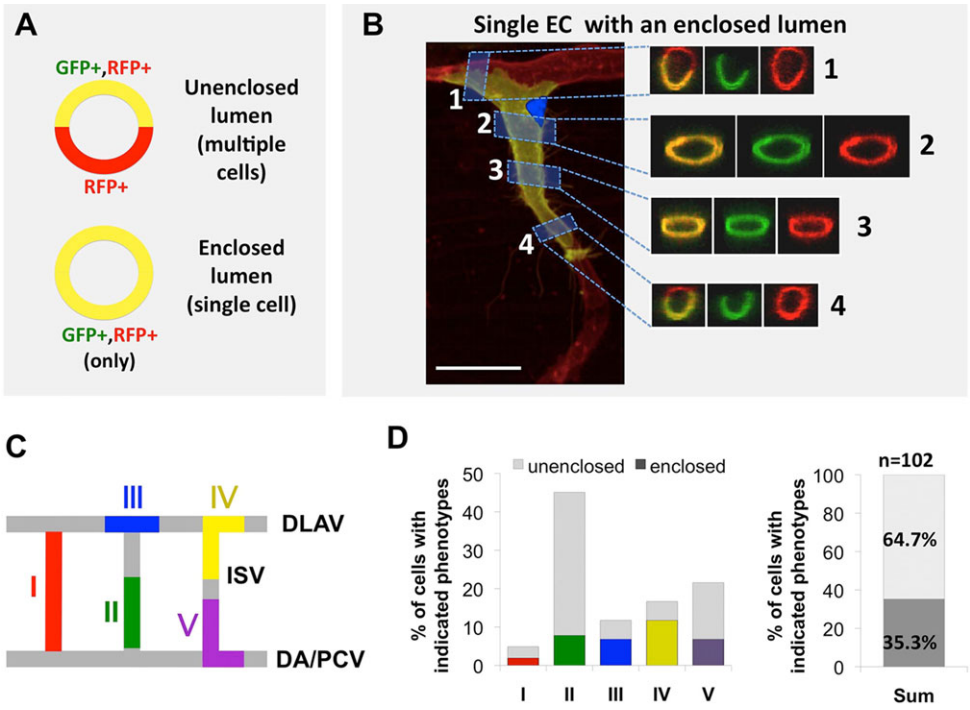

Fig. 5. Endothelial lumen heterogeneity revealed by single-cell 3D reconstruction. (A) Schematics showing potential configurations of verified single *Tol2 (fli1a:H2B-TagBFP-p2A-egfp-F)* transgene-expressing ECs adjoining lumenal spaces, in cross-sections of vessels containing these cells from transgene-injected *Tg(kdrl:mRFP-F)*^{y286} embryos. Unenclosed lumen: if multiple cells enclose a lumen segment (top), both GFP/RFP double-positive (expressing the injected transgene) and RFP single-positive (not expressing the injected transgene) sectors of the vessel will be detected (see B, 1 and 4). Enclosed lumen: if only a single cell encloses a lumen segment (bottom), the vessel wall will be entirely GFP/RFP double positive (expressing the injected transgene; see B, 2 and 3). (B) Confocal images of a verified single *Tol2(fli1a:H2B-TagBFP-p2A-egfp-F)* transgene-expressing EC (yellow) in the dorsal part of a *Tg(kdrl:mRFP-F)*^{y286} vessel (red). The left panel shows a lateral view reconstruction of the entire cell, with the single nucleus visible by blue fluorescence. To the right are red/green merge (left), green and red fluorescence images of four image slices. Slices 1 and 4 show lumens bounded by both the injected transgenic EC and other EC(s). Slices 2 and 3 show lumens bounded by only the single injected transgene-positive EC. (C) Morphological classification of ECs contributing to the ISV/DLAV (see Fig. 3 for details). (D) Quantification of the proportion of ECs with unenclosed (gray) or enclosed (colored) lumen found in each of the five morphological classes and in total combined trunk ECs. Scale bar: 20 µm.

junctions. To address this issue, we developed a genetic approach to label EC junctions *in vivo* using fluorescent proteins. A fusion protein construct was generated (Fig. 6B) using the coding sequences for the endothelial-specific tight junction protein Claudin 5b and eGFP. This construct was placed under the control of the endothelial *fli1a* promoter in a Tol2 vector, and stable double germline transgenic *Tg(fli1a:egfp-claudin 5b)*^{y287}*; Tg (kdrl:mRFP-F)*^{y286} animals were generated. The *Tg(fli1a:egfp-claudin 5b)*^{y287}*; Tg(kdrl:mRFP-F)*^{y286} double-transgenic animals, and the vessels within them, develop indistinguishably from those of *Tg(kdrl:mRFP-F)*^{y286} control animals. The eGFP-Claudin 5b fusion protein colocalizes with endogenous ZO-1 (Tjp1a – ZFIN), as shown by co-immunostaining with anti-eGFP and anti-ZO-1 antibodies (supplementary material Fig. S4), validating that this transgenic line permits detailed visualization of EC tight junction complexes in living animals (Fig. 6C,D).

We carried out extensive confocal and two-photon microscopy using this line to examine the junctional morphology of the newly assembled ISVs and DLAVs in the trunk of zebrafish embryos. We were able to identify a variety of junctional types suggestive of different types of EC-EC contacts in these vessels (Fig. 6D-G; supplementary material Movies 2-4). Interestingly, we found that approximately one-quarter of the length of all vessel segments lacked any obvious junctions (Fig. 6E,H,I; supplementary material Movie 2). The proportion of vessel length lacking eGFP-Claudin 5b junctional localization was greater in the DLAV (34.9±7.7%) than in the ascending ISV (17.9±5.6%). These ‘gaps’ in junctional localization along the vessels were not a result of lack of transgene expression in selected cells, as the gaps were also observed in mosaics generated by injecting a *Tol2(kdrl:mcherry-p2A-egfp-claudin 5b)* transgene simultaneously labeling EC bodies and tight junctions. In these animals approximately one-quarter of the length of transgene-labeled ECs showed ‘dark’ gaps in eGFP-Claudin 5b fusion protein localization despite expressing mCherry throughout the cell (Fig. 6J-M; supplementary material Movie 5). 3D examination of eGFP-Claudin 5b patterns in these mosaics also revealed the complexity of endothelial junctional morphology and the difficulty in interpreting morphology from static single-view images (compare supplementary material Movie 5 and Fig. 6M). Tight junction-free vessel segments are also detected by endogenous ZO-1 staining in the perfused ISV and DLAV (supplementary material Fig. S4). Tight junction-free vessel segments in *Tg(fli1a:egfp-claudin 5b)*^{y287}*; Tg(kdrl:mRFP-F)*^{y286} double-transgenic animals persist for at least a day after ISV lumenization (supplementary material Fig. S5A-C), showing that these are not simply transient intermediates during vessel formation, although the overall length of these segments does decrease over time (supplementary material Fig. S5D,E).

Together, our results suggest that, at least for small-caliber early trunk vessels (ISV, DLAV), there are multiple types of tubular lumens and cell junction distributions, with lumens either hollowed inside the cell, enclosed by a single EC, or sealed by multiple ECs

Development (2015) 142, 2951-2961 doi:10.1242/dev.123174

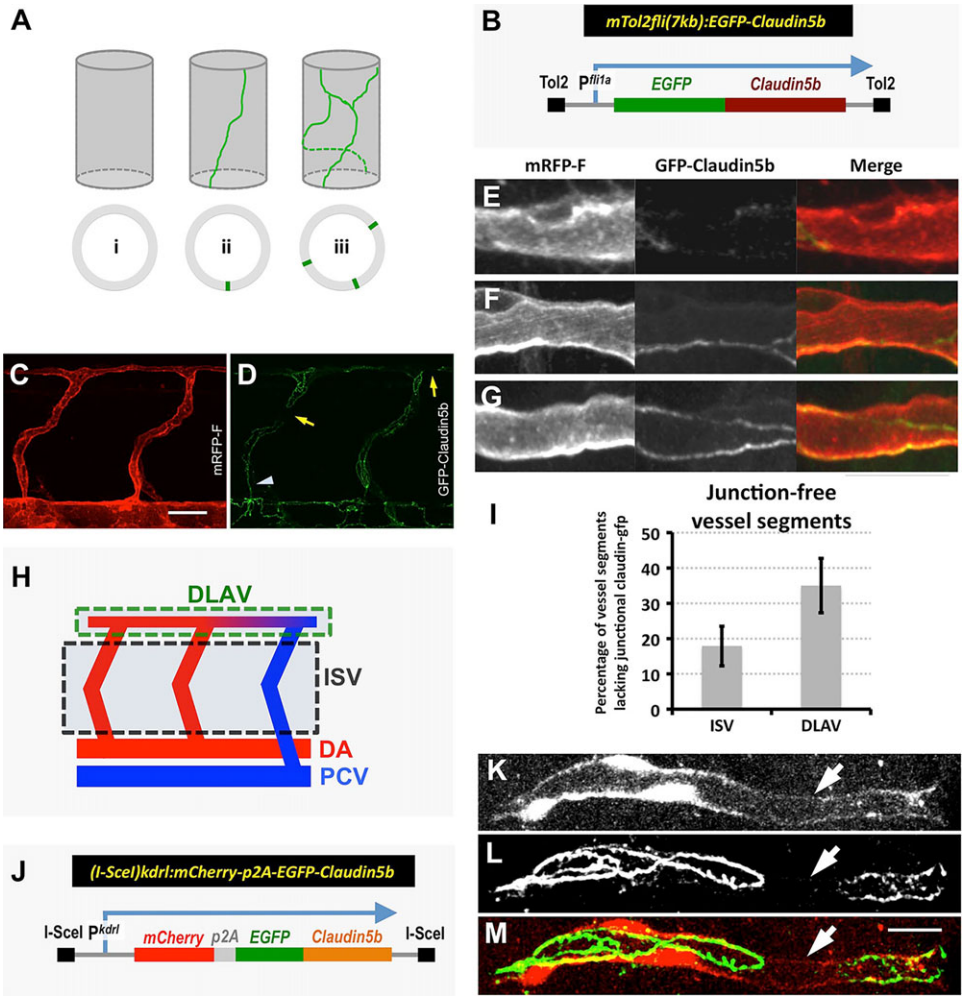

Fig. 6. *In vivo* imaging of EC junctions. (A) Schematic depicting representative junctional morphologies observed in a unicellular endothelial 'seamless' tube lacking junctions along its length (i), a unicellular endothelial tube forming an autocellular junction (ii), and a multicellular endothelial tube with multiple intercellular junctions (iii). (B) Diagram of the *Tg(fli1a:egfp-claudin 5b)* Tol2 transgene construct used for generating a stable transgenic line marking endothelial junctions. (C,D) Confocal images of mid-trunk vessels in 42 hpf *Tg(fli1a:egfp-claudin 5b)*^{y287}*; Tg(kdrl:mRFP-F)*^{y286} double-transgenic embryos, showing eGFP-labeled endothelial tight junctions (D, green) in mRFP-positive ECs (C, red). Blood vessel segments with either no eGFP-Claudin 5b-labeled tight junction or a single line of eGFP-Claudin 5b-labeled tight junctions are highlighted by arrows or arrowhead, accordingly. (E-G) Higher magnification confocal micrographs of mid-trunk vessels in 48 hpf *Tg(fli1a:egfp-claudin 5b)*^{y287}*; Tg(kdrl:mRFP-F)* ^{y286} double-transgenic embryos, showing vessel segments with a 'gap' in eGFP-Claudin 5b expression (E), with a single line of eGFP-Claudin 5b (F), and with multiple lines of eGFP-Claudin 5b (G). 3D rotations of the merged images in E-G are shown in supplementary material Movies 2-4. (H) Schematic of the trunk vascular network, showing ascending ISV and dorsal DLAV vascular segments that are quantified for the presence or absence of junctions (localized eGFP-Claudin 5b) in I. Arterial vessels (dorsal aorta, intersegmental arteries) are shown in red, venous vessels (posterior cardinal vein, intersegmental veins) are show in blue, and arterial-venous transition zones in the DLAV are denoted with a red-blue gradient. (I) Quantification of the percentage of vessel segments lacking localized eGFP-Claudin 5b expression in the ascending ISV segments or dorsal DLAV segments. (J) Diagram of the *Tg(kdrl1:mcherry-p2A-egfp-claudin 5b)* I-SceI *kdrl* transgene construct used for mosaic colabeling of EC membranes (mCherry) and cell-cell junctions (eGFP-Claudin 5b). (K-M) Higher magnification confocal micrographs of a 48 hpf embryo injected with a *Tol2(kdrl:mcherry-p2A-egfp-claudin 5b)* transgene, showing mCherry (K), eGFP (L) and merged (M) fluorescence images. The mCherry-positive segment (K) has eGFP-Claudin 5b (L) localized to the ends but an eGFP-Claudin 5b-negative gap in the center of the segment (arrow). A 3D rotation of the merged image in M is shown in supplementary material Movie 5. All images are lateral views with rostral to the left. Scale bars: 20 µm in C,D; 10 µm in K-M.

(Fig. 6A). These observations, in concert with the results from single EC 3D configuration analysis, suggest that multiple mechanisms of lumen formation coexist in the early developing vasculature.

Intracellular vacuoles within individual ECs are likely to contribute to initial lumenization

Our laboratory and others have previously reported intracellular vacuoles contributing to lumen formation *in vitro* and *in vivo* (Bayless and Davis, 2002; Davis et al., 2011; Folkman and Haudenschild, 1980a; Kamei et al., 2006; Koh et al., 2009; Sacharidou et al., 2012). However, other recent work has highlighted the importance of cellular rearrangements and multicellular/extracellular lumenization (Wacker and Gerhardt, 2011), and the existence of intracellular vacuoles or nascent lumenal compartments has been questioned. This is in part because of the challenges in imaging these compartments *in vivo* and the difficulty of discerning whether these spaces are found within single ECs or between multiple ECs.

In order to examine whether intracellular vacuoles are present during ISV/DLAV assembly, we used two-photon imaging to visualize subcellular compartments in single *Tol2(fli1a:h2b-tagBFP-2A-egfp-f)* ECs in *Tg(kdrl:mRFP-F)*^{y286} animals. Using the *h2b-tagBFP* tag to verify that we were indeed examining single

Development (2015) 142, 2951-2961 doi:10.1242/dev.123174

ECs, we were able to observe eGFP-farnesyl-labeled intracellular membrane structures of varying sizes that appeared to be entirely enclosed within the cytoplasm (Fig. 7A,B; supplementary material Movies 6 and 7). These were observed frequently within individual ECs, especially at the early stages before lumen formation. Using time-lapse imaging we were also able to observe fusion of multiple smaller vesicles to generate larger vacuolar compartments within single ECs (Fig. 7C,D; supplementary material Movie 8). We were also able to image the emergence of a vacuolar compartment that appeared to be enclosed within a single EC and its subsequent enlargement and eventual fusion with the nascent adjacent extracellular space (supplementary material Fig. S6, Movie 9). Intracellular vesicular/vacuolar compartments were observed more frequently in the unlumenized tip cells than in lumen-forming stalk cells.

Taken together with our results showing an increased proportion of seamless vessel segments in the newly formed DLAV, these findings suggest that intracellular membrane-bound compartments may contribute to the initial lumenization of angiogenic trunk vessels.

DISCUSSION

Developmental angiogenesis is a tightly controlled process that involves complex and diverse endothelial cellular behaviors. Over the past decade, a great deal of effort has been focused on understanding the molecular mechanisms regulating angiogenesis, but most of this work has been carried out using *in vitro* EC culture methods or by studying vessels *in vivo* at the tissue level. Our understanding of the cellular mechanisms regulating angiogenesis *in vivo* remains incomplete, at least in part due to the limitations of live imaging of ECs *in vivo* and lack of suitable genetic tools for analyzing the morphology and behavior of individual ECs in the context of the entire vasculature. Although studies of vessel formation at the organ and tissue levels have provided important insights into the underlying genetic basis for embryonic vascular development and organogenesis, endothelial morphology and/or dynamics have mostly been analyzed in groups of ECs or whole growing vessels rather than in individual ECs, which generally cannot be definitively distinguished from their neighbors.

In this study, we describe an approach for labeling and definitively identifying single ECs *in vivo*. We prepared transgene constructs driving simultaneous expression of a blue fluorescent tag in EC nuclei (H2B-TagBFP), to definitively identify individual cells by their nuclei, and a green fluorescent tag in EC membranes (eGFP-F), to visualize cellular and subcellular morphology. The H2B-TagBFP and eGFP-F proteins are stoichiometrically coexpressed from the same construct by linking them together using a viral 2A peptide sequence (Kim et al., 2011) permitting co-translational expression of both proteins (Provost et al., 2007; Wang et al., 2011). Injection of the *Tol2 (fli1a:h2b-tagBFP-2A-egfp-f)* transgene into *Tg(kdrl:mRFP-F)*^{y286} germline transgenic zebrafish results in mosaic coexpression of H2B-TagBFP and eGFP-F in a subset of ECs within globally mRFP-F-positive vasculature. By examining the nuclear H2B-TagBFP and cellular eGFP-F expression in the ECs of mosaic injected animals, it is straightforward to identify individually tagged ECs for morphological and behavioral characterization that have no immediately adjacent tagged neighbors. This makes it possible to examine the morphology and behavior of individual ECs within the context of multicellular vascular cords or tubes.

As a proof-of-principle to demonstrate the usefulness of this method for qualitative and quantitative analysis of differences in EC morphology and behavior between normal and defective vasculature, we carried out single EC analysis in Plxnd1-deficient embryos. In previous studies, we and others have shown that growing ISVs lacking the endothelial-specific semaphorin receptor Plxnd1 due to genetic mutation or knockdown are unable to respond to somite-derived semaphorin guidance cues that normally restrict their growth to intersomitic boundaries, resulting in loss of proper directionality in their growth and the formation of disorganized trunk vascular networks (Gitler et al., 2004; Gu et al., 2005; Torres-Vazquez et al., 2004). By measuring the amount and dynamics of membrane protrusions in individual

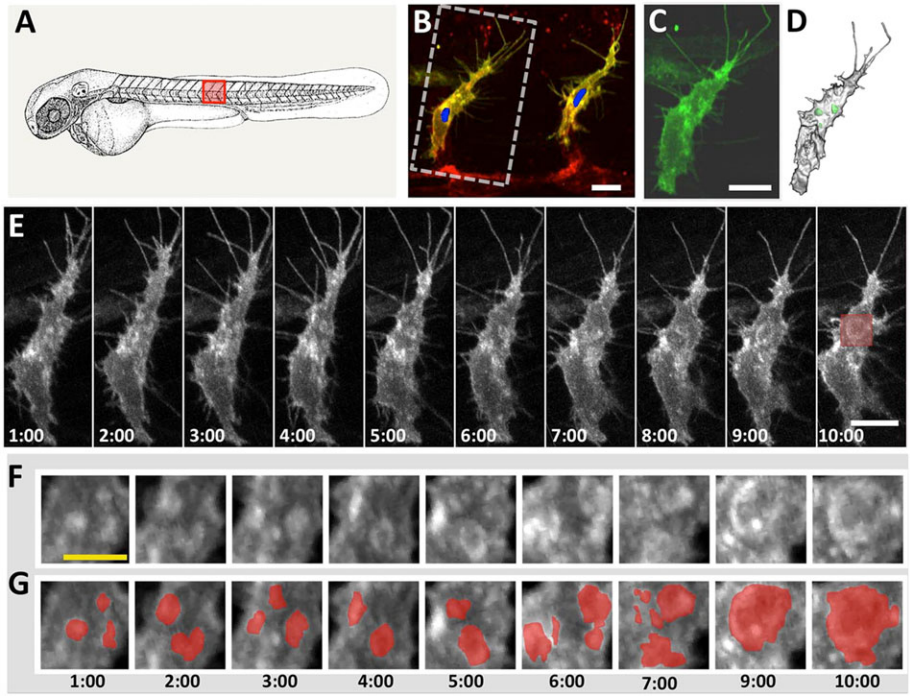

Fig. 7. Single-cell analysis of intracellular vacuole fusion during vascular lumenization. (A) Schematic of a zebrafish embryo showing the position of the trunk vessels in B. (B) Confocal micrograph of a verified single *Tol2(fli1a:H2B-TagBFP-p2A-egfp-F)* transgene-expressing EC in the trunk of an ~28 hpf *Tg(kdrl:mRFP-F)*^{y286} embryo. (C) A single cell (boxed in B) was chosen for time-lapse analysis. (D) Surface-rendered 3D reconstruction of an image stack collected of the cell in C, with intracellular compartments highlighted in green (see supplementary material Movies 7 and 8 for a 3D rotation of the reconstruction and the deconvolved image stack, respectively). (E) Confocal micrograph time series of a verified single *Tol2(fli1a:H2B-TagBFP-p2A-egfp-F)* transgene-expressing EC in the trunk of a ~30 hpf *Tg(kdrl:mRFP-F)*^{y286} embryo. (F,G) Magnified images of the boxed region in E, with intracellular vesicular/vacuolar compartments highlighted in red in G. Scale bar: 10 µm in B,C,E; 5 µm in F.

Development (2015) 142, 2951-2961 doi:10.1242/dev.123174

trunk ECs we were able to show that, although the total length of endothelial protrusions is similar in control and *plxnd1* morpholino-injected animals, the directionality of protrusions is altered. Our results also revealed a prolonged persistence of endothelial membrane protrusions in *plxnd1* morphants compared with controls, as might be expected given the inability of these ECs to respond to repulsive semaphorin cues produced by the adjacent somites. A similar prolongation of protrusions has been noted in axonal growth cones in the absence of semaphorin-plexin repulsion (Ayoob et al., 2004; Chauvet et al., 2007).

Vascular lumen formation is a complicated morphogenetic process involving the structural transition from a cord of ECs to a hollow tube. As discussed in detail in the introduction, recent reports have highlighted a number of different mechanisms potentially involved in endothelial tubulogenesis (Charpentier and Conlon, 2014). It has been proposed that vascular tubes form via either cord hollowing, involving cellular rearrangements, or cell hollowing, involving the formation and fusion of intracellular vacuoles (Charpentier and Conlon, 2014; Ellertsdottir et al., 2010; Kamei et al., 2006; Lampugnani et al., 2010; Lubarsky and Krasnow, 2003; Strilic et al., 2009; Wang et al., 2010). Mechanisms such as adhesion to surrounding ECM, loss of EC-EC contacts, repulsive interaction between EC surfaces, and the formation of intracellular vacuoles and their intra- or intercellular fusion have all been suggested as important forces promoting the expansion of nascent lumenal spaces. The cellular basis for endothelial tube formation *in vivo* has been difficult to study due to the challenge of observing individual EC behaviors within the vasculature. Our single-cell analysis in intact live animals suggests that endothelial tube formation occurs in a heterogeneous manner, using a combination of different cellular mechanisms (Fig. 8). We observe both single-cell-enclosed lumens and lumens lined by multiple ECs within newly formed tubes in the trunk vascular network. Live imaging of EC junctions reveals that many lumenal segments enclosed by single ECs lack apparent autocellular junctions, suggesting that these are seamless vascular tubes formed, at least in part, by a cell hollowing mechanism. The existence of seamless vascular tubes in mammals has also been suggested from electron microscopy analysis of capillary vessels from various vascular beds (Bar et al., 1984) and by VE-cadherin staining of the mouse retinal vasculature (Ehling et al., 2013; Fan et al., 2014). We also document the existence of small vesicles and larger vacuoles within individual ECs of angiogenic ISVs, although additional work will be needed to definitively conclude whether these vacuole-like structures fuse and enlarge intracellularly, directly form extracellular spaces between adjacent ECs, or a combination of both. Taken together, our observations and those of many other groups using a variety of different approaches strongly suggest that angiogenic sprouts, especially those forming small-caliber vessels such as capillaries, become lumenized through multiple distinct cellular mechanisms including both cord hollowing and cell hollowing. The coexistence of multiple cellular mechanisms for lumen formation might be advantageous for endothelial adaptation to the local challenges of distinct microenvironments.

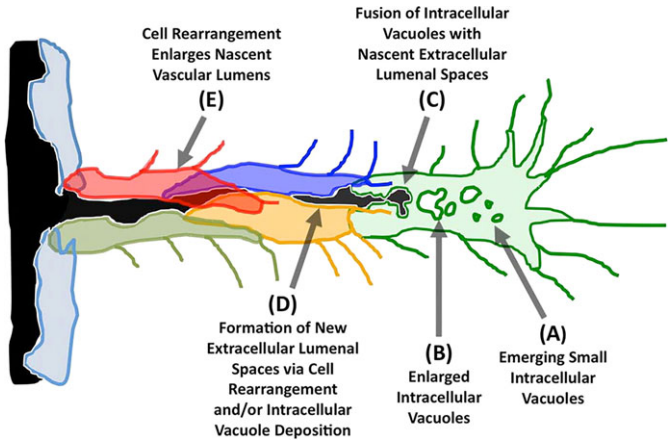

Fig. 8. Proposed mechanisms contributing to lumen formation during trunk vessel formation. Vascular lumens and nascent extracellular lumenal spaces are shown in solid black, ECs are shown in semi-transparent colors. (A) Small intracellular vacuoles emerge in ECs of growing vascular segments, most prominently in leading or 'tip' cells. (B) Smaller vacuolar compartments merge and/or grow to form larger intracellular compartments. (C) Intracellular vacuoles eventually fuse with the plasma membrane and merge with nascent extracellular lumenal spaces. (D) Extracellular nascent lumenal spaces can also form via cellular rearrangement (either single-cell self-lumenization or multicellular lumenization), most probably in conjunction with lumenal enlargement via extracellular deposition of intracellular vacuoles, as in C. (E) Further cell rearrangement occurs to enlarge the lumen and stabilize the mature vascular tube. Lumenization via cell rearrangement and via vacuoles are likely to occur together throughout this process.

EC abnormalities in form and function are common features of many conditions involving pathological angiogenesis, notably cancer (Baluk et al., 2005). Although there has been enormous progress recently in identifying the genetic and epigenetic factors that contribute to changes in blood vessel form and function at the tissue level, a thorough investigation of the underlying *in vivo* cellular mechanisms at high resolution is needed to understand how molecular alterations in ECs translate into changes in the vasculature at the tissue level. The new tools that we describe here should be useful in helping to bridge this knowledge gap.

MATERIALS AND METHODS

Zebrafish

Zebrafish were maintained and zebrafish experiments were performed according to standard protocols (Westerfield, 2000) and in conformity with the Guide for the Care and Use of Laboratory Animals of National Institutes of Health in an Association for Assessment and Accreditation of Laboratory Animal Care (AAALAC) accredited facility. Wild-type EK strain was obtained through natural spawning from Ekkwill (Ruskin, FL, USA). All transgenic lines were maintained in the EK strain. Transgenic lines *Tg(fli1a:nls-egfp)*^{y7} and *Tg(kdrl:mcherry-caax)*^{y171} were published previously (Fujita et al., 2011; Siekmann and Lawson, 2007).

Plasmid constructs and morpholinos

For plasmid Tol2fli1a:H2B-TagBFP-p2A-eGFP-F, TagBFP-tagged human histone H2B was purchased from Evrogen (pTagBFP-H2B, #FP176); porcine 2A viral peptide (DNA sequence: 5′-GGAAGCGGAGCTACTA-ACTTCAGCCTGCTGAAGCAGGCTGGAGACGTGGAGGAGAACC-CTGGACCT-3′) was fused between TagBFP-H2B and eGFP-farnesyl sequences; then H2B-TagBFP-p2A-eGFP-F was subcloned into miniTol2-containing vector harboring the endothelial promoter *fli1a*.

The zebrafish *claudin 5b* gene (NCBI accession NM_001006044) was amplified from a cDNA library from 48 hours post-fertilization (hpf) zebrafish embryos. *claudin 5b* was subcloned into pEGFP-C1 (Kamei et al., 2006) to generate eGFP-Claudin 5b. eGFP-Claudin 5b was digested by *Nhe*I and *Mlu*I and subcloned into miniTol2-containing vector harboring the endothelial promoter *fli1a*. For plasmid (I-SceI) kdrl:mCherry-p2A-eGFP-Claudin 5b, the constructs p5′E:mCherry-p2A, pME:eGFP-Claudin 5b and p3′E:polyA were cloned into vector pDEST:kdrl (Fujita et al., 2011) containing meganuclease I-*Sce*I sequences using a MultiSite Gateway Construction Kit (Invitrogen).

Development (2015) 142, 2951-2961 doi:10.1242/dev.123174

Morpholinos targeting *plxnd1* (5′-TGAGGGTATTTACAGTCGCTCC-GC-3′) were injected at the one- to four-cell stage at a dose of 5 ng (Torres-Vazquez et al., 2004).

Mosaic analysis and germline transgenesis

For mosaic single-cell analysis, 1 nl solution containing 25 ng/µl Tol2fli1a:H2B-TagBFP-p2A-eGFP-F DNA plasmid and 30 ng/µl miniTol2 RNA was injected into *Tg(kdrl:mRFP-F)*^{y286} transgenic embryos at the one-cell stage. Injected embryos with membrane GFP fluorescence in the developing vasculature were selected for single EC morphology analysis under two-photon confocal microscopy. For stable transgenic germline generation, Tol2fli1a:eGFP-Claudin 5b or ISceIkdrl:mRFP-F DNA plasmid was co-injected with miniTol2 RNA or I-*Sce*I meganuclease protein into wild-type EK embryos at the one-cell stage. Embryos with fluorescent blood vessels were selected as F0 founders and maintained for descendant generations.

Microscopy and image processing

Live embryos were mounted in 0.7% low-melting agarose gel and cultured in embryo water for confocal imaging using a long working distance objective (20×, water-immersion, 507701, Leica). Confocal images were acquired with a FluoView 1000 (Olympus) or TCS SP5II (Leica) confocal microscope equipped with an imaging chamber mounted with MatTek 60 mm glass-bottom dishes. *z*-series stacks were captured with 0.25 µm spacing between image planes. The active contour-based image segmentation and 3D reconstruction were performed using Volocity 6.0 (PerkinElmer) and Imaris 7.4 (Bitplane) software. 3D rotation movies were constructed using ImageJ (NIH) and MAYA (Autodesk). Lasers used in this study: 850 nm 2P for TagBFP, 488 nm for eGFP, 561 nm argon laser for mRFP and mCherry.

Statistical analysis

Statistical analysis was performed using Prism 6.0 (GraphPad). Box-and-whisker with minimum and maximum and geometric plots with mean±s.d. were generated from Prism graphs. The difference among indicated groups was evaluated by unpaired two-tailed Student's *t*-test. $P<0.05$ was considered as statistically significant between test groups. Polar graphs for filopodia protrusiveness and spatial distribution were generated by open-source software Gnumeric 1.12.16 (www.gnumeric.org).

Acknowledgements

We thank members of the B.M.W. laboratory for technical help and critical suggestions; Dr Roberto Weigert for providing XFP-F constructs; Ms Jingjing Wang for help in generating transgenic fish; and Jeremy Swan and Sam Farabaugh for assistance with image processing.

Competing interests

The authors declare no competing or financial interests.

Author contributions

J.A.Y. and B.M.W. designed the experiments, analyzed the data and wrote the manuscript. J.A.Y. performed the experiments with help from D.C. and V.N.P.

Funding

This study was supported by the intramural program of the Eunice Kennedy Shriver National Institute of Child Health and Human Development at the National Institutes of Health [ZIA-HD001011], and by the Leducq Foundation. Deposited in PMC for release after 12 months.

Supplementary material

Supplementary material available online at
http://dev.biologists.org/lookup/suppl/doi:10.1242/dev.123174/-/DC1

References

Aird, W. C. (2007a). Phenotypic heterogeneity of the endothelium: I. Structure, function, and mechanisms. *Circ. Res.* **100**, 158-173.

Aird, W. C. (2007b). Phenotypic heterogeneity of the endothelium: II. Representative vascular beds. *Circ. Res.* **100**, 174-190.

Aird, W. C. (2012). Endothelial cell heterogeneity. *Cold Spring Harb. Perspect. Med.* **2**, a006429.

Ayoob, J. C., Yu, H.-H., Terman, J. R. and Kolodkin, A. L. (2004). The Drosophila receptor guanylyl cyclase Gyc76C is required for semaphorin-1a-plexin A-mediated axonal repulsion. *J. Neurosci.* **24**, 6639-6649.

Baluk, P., Hashizume, H. and McDonald, D. M. (2005). Cellular abnormalities of blood vessels as targets in cancer. *Curr. Opin. Genet. Dev.* **15**, 102-111.

Bar, T., Guldner, F.-H. and Wolff, J. R. (1984). "Seamless" endothelial cells of blood capillaries. *Cell Tissue Res.* **235**, 99-106.

Bayless, K. J. and Davis, G. E. (2002). The Cdc42 and Rac1 GTPases are required for capillary lumen formation in three-dimensional extracellular matrices. *J. Cell Sci.* **115**, 1123-1136.

Bayless, K. J., Salazar, R. and Davis, G. E. (2000). RGD-dependent vacuolation and lumen formation observed during endothelial cell morphogenesis in three-dimensional fibrin matrices involves the alpha(v)beta(3) and alpha(5)beta(1) integrins. *Am. J. Pathol.* **156**, 1673-1683.

Butler, M. G., Gore, A. V. and Weinstein, B. M. (2011). Zebrafish as a model for hemorrhagic stroke. *Methods Cell Biol.* **105**, 137-161.

Charpentier, M. S. and Conlon, F. L. (2014). Cellular and molecular mechanisms underlying blood vessel lumen formation. *BioEssays* **36**, 251-259.

Chauvet, S., Cohen, S., Yoshida, Y., Fekrane, L., Livet, J., Gayet, O., Segu, L., Buhot, M.-C., Jessell, T. M., Henderson, C. E. et al. (2007). Gating of Sema3E/PlexinD1 signaling by neuropilin-1 switches axonal repulsion to attraction during brain development. *Neuron* **56**, 807-822.

Chung, A. S. and Ferrara, N. (2011). Developmental and pathological angiogenesis. *Annu. Rev. Cell Dev. Biol.* **27**, 563-584.

Davis, G. E., Stratman, A. N., Sacharidou, A. and Koh, W. (2011). Molecular basis for endothelial lumen formation and tubulogenesis during vasculogenesis and angiogenic sprouting. *Int. Rev. Cell Mol. Biol.* **288**, 101-165.

del Toro, R., Prahst, C., Mathivet, T., Siegfried, G., Kaminker, J. S., Larrivee, B., Breant, C., Duarte, A., Takakura, N., Fukamizu, A. et al. (2010). Identification and functional analysis of endothelial tip cell-enriched genes. *Blood* **116**, 4025-4033.

Egginton, S. and Gerritsen, M. (2003). Lumen formation in vivo versus in vitro observations. *Microcirculation* **10**, 45-61.

Ehling, M., Adams, S., Benedito, R. and Adams, R. H. (2013). Notch controls retinal blood vessel maturation and quiescence. *Development* **140**, 3051-3061.

Eilken, H. M. and Adams, R. H. (2010). Dynamics of endothelial cell behavior in sprouting angiogenesis. *Curr. Opin. Cell Biol.* **22**, 617-625.

Ellertsdottir, E., Lenard, A., Blum, Y., Krudewig, A., Herwig, L., Affolter, M. and Belting, H.-G. (2010). Vascular morphogenesis in the zebrafish embryo. *Dev. Biol.* **341**, 56-65.

Fan, J., Ponferrada, V. G., Sato, T., Vemaraju, S., Fruttiger, M., Gerhardt, H., Ferrara, N. and Lang, R. A. (2014). Crim1 maintains retinal vascular stability during development by regulating endothelial cell Vegfa autocrine signaling. *Development* **141**, 448-459.

Folkman, J. and Haudenschild, C. (1980a). Angiogenesis by capillary endothelial cells in culture. *Trans. Ophthalmol. Soc. UK* **100**, 346-353.

Folkman, J. and Haudenschild, C. (1980b). Angiogenesis in vitro. *Nature* **288**, 551-556.

Fujita, M., Cha, Y. R., Pham, V. N., Sakurai, A., Roman, B. L., Gutkind, J. S. and Weinstein, B. M. (2011). Assembly and patterning of the vascular network of the vertebrate hindbrain. *Development* **138**, 1705-1715.

Gerhardt, H., Golding, M., Fruttiger, M., Ruhrberg, C., Lundkvist, A., Abramsson, A., Jeltsch, M., Mitchell, C., Alitalo, K., Shima, D. et al. (2003). VEGF guides angiogenic sprouting utilizing endothelial tip cell filopodia. *J. Cell Biol.* **161**, 1163-1177.

Gitler, A. D., Lu, M. M. and Epstein, J. A. (2004). PlexinD1 and semaphorin signaling are required in endothelial cells for cardiovascular development. *Dev. Cell* **7**, 107-116.

Gore, A. V., Monzo, K., Cha, Y. R., Pan, W. and Weinstein, B. M. (2012). Vascular development in the zebrafish. *Cold Spring Harb. Perspect. Med.* **2**, a006684.

Gu, C., Yoshida, Y., Livet, J., Reimert, D. V., Mann, F., Merte, J., Henderson, C. E., Jessell, T. M., Kolodkin, A. L. and Ginty, D. D. (2005). Semaphorin 3E and plexin-D1 control vascular pattern independently of neuropilins. *Science* **307**, 265-268.

Herbert, S. P. and Stainier, D. Y. R. (2011). Molecular control of endothelial cell behaviour during blood vessel morphogenesis. *Nat. Rev. Mol. Cell Biol.* **12**, 551-564.

Herwig, L., Blum, Y., Krudewig, A., Ellertsdottir, E., Lenard, A., Belting, H.-G. and Affolter, M. (2011). Distinct cellular mechanisms of blood vessel fusion in the zebrafish embryo. *Curr. Biol.* **21**, 1942-1948.

Iruela-Arispe, M. L. and Beitel, G. J. (2013). Tubulogenesis. *Development* **140**, 2851-2855.

Iruela-Arispe, M. L. and Davis, G. E. (2009). Cellular and molecular mechanisms of vascular lumen formation. *Dev. Cell* **16**, 222-231.

Isogai, S., Lawson, N. D., Torrealday, S., Horiguchi, M. and Weinstein, B. M. (2003). Angiogenic network formation in the developing vertebrate trunk. *Development* **130**, 5281-5290.

Jakobsson, L., Franco, C. A., Bentley, K., Collins, R. T., Ponsioen, B., Aspalter, I. M., Rosewell, I., Busse, M., Thurston, G., Medvinsky, A. et al. (2010). Endothelial cells dynamically compete for the tip cell position during angiogenic sprouting. *Nat. Cell Biol.* **12**, 943-953.

Jin, S.-W., Beis, D., Mitchell, T., Chen, J.-N. and Stainier, D. Y. R. (2005). Cellular and molecular analyses of vascular tube and lumen formation in zebrafish. *Development* **132**, 5199-5209.
Jin, S.-W., Herzog, W., Santoro, M. M., Mitchell, T. S., Frantsve, J., Jungblut, B., Beis, D., Scott, I. C., D'Amico, L. A., Ober, E. A. et al. (2007). A transgene-assisted genetic screen identifies essential regulators of vascular development in vertebrate embryos. *Dev. Biol.* **307**, 29-42.
Kalen, M., Wallgard, E., Asker, N., Nasevicius, A., Athley, E., Billgren, E., Larson, J. D., Wadman, S. A., Norseng, E., Clark, K. J. et al. (2009). Combination of reverse and chemical genetic screens reveals angiogenesis inhibitors and targets. *Chem. Biol.* **16**, 432-441.
Kamei, M., Saunders, W. B., Bayless, K. J., Dye, L., Davis, G. E. and Weinstein, B. M. (2006). Endothelial tubes assemble from intracellular vacuoles in vivo. *Nature* **442**, 453-456.
Kim, J. H., Lee, S.-R., Li, L.-H., Park, H.-J., Park, J.-H., Lee, K. Y., Kim, M.-K., Shin, B. A. and Choi, S.-Y. (2011). High cleavage efficiency of a 2A peptide derived from porcine teschovirus-1 in human cell lines, zebrafish and mice. *PLoS ONE* **6**, e18556.
Koh, W., Stratman, A. N., Sacharidou, A. and Davis, G. E. (2008). In vitro three dimensional collagen matrix models of endothelial lumen formation during vasculogenesis and angiogenesis. *Methods Enzymol.* **443**, 83-101.
Koh, W., Sachidanandam, K., Stratman, A. N., Sacharidou, A., Mayo, A. M., Murphy, E. A., Cheresh, D. A. and Davis, G. E. (2009). Formation of endothelial lumens requires a coordinated PKCepsilon-, Src-, Pak- and Raf-kinase-dependent signaling cascade downstream of Cdc42 activation. *J. Cell Sci.* **122**, 1812-1822.
Lampugnani, M. G., Orsenigo, F., Rudini, N., Maddaluno, L., Boulday, G., Chapon, F. and Dejana, E. (2010). CCM1 regulates vascular-lumen organization by inducing endothelial polarity. *J. Cell Sci.* **123**, 1073-1080.
Lawson, N. D. and Weinstein, B. M. (2002). In vivo imaging of embryonic vascular development using transgenic zebrafish. *Dev. Biol.* **248**, 307-318.
Lenard, A., Ellertsdottir, E., Herwig, L., Krudewig, A., Sauteur, L., Belting, H.-G. and Affolter, M. (2013). In vivo analysis reveals a highly stereotypic morphogenetic pathway of vascular anastomosis. *Dev. Cell* **25**, 492-506.
Lubarsky, B. and Krasnow, M. A. (2003). Tube morphogenesis: making and shaping biological tubes. *Cell* **112**, 19-28.
Nolan, D. J., Ginsberg, M., Israely, E., Palikuqi, B., Poulos, M. G., James, D., Ding, B.-S., Schachterle, W., Liu, Y., Rosenwaks, Z. et al. (2013). Molecular signatures of tissue-specific microvascular endothelial cell heterogeneity in organ maintenance and regeneration. *Dev. Cell* **26**, 204-219.
Pelton, J. C., Wright, C. E., Leitges, M. and Bautch, V. L. (2014). Multiple endothelial cells constitute the tip of developing blood vessels and polarize to promote lumen formation. *Development* **141**, 4121-4126.
Phng, L.-K., Stanchi, F. and Gerhardt, H. (2013). Filopodia are dispensable for endothelial tip cell guidance. *Development* **140**, 4031-4040.
Popson, S. A., Ziegler, M. E., Chen, X., Holderfield, M. T., Shaaban, C. I., Fong, A. H., Welch-Reardon, K. M., Papkoff, J. and Hughes, C. C. W. (2014). Interferon-induced transmembrane protein 1 regulates endothelial lumen formation during angiogenesis. *Arterioscler. Thromb. Vasc. Biol.* **34**, 1011-1019.
Provost, E., Rhee, J. and Leach, S. D. (2007). Viral 2A peptides allow expression of multiple proteins from a single ORF in transgenic zebrafish embryos. *Genesis* **45**, 625-629.
Sacharidou, A., Koh, W., Stratman, A. N., Mayo, A. M., Fisher, K. E. and Davis, G. E. (2010). Endothelial lumen signaling complexes control 3D matrix-specific tubulogenesis through interdependent Cdc42- and MT1-MMP-mediated events. *Blood* **115**, 5259-5269.
Sacharidou, A., Stratman, A. N. and Davis, G. E. (2012). Molecular mechanisms controlling vascular lumen formation in three-dimensional extracellular matrices. *Cells Tissues Organs* **195**, 122-143.
Siekmann, A. F. and Lawson, N. D. (2007). Notch signalling limits angiogenic cell behaviour in developing zebrafish arteries. *Nature* **445**, 781-784.
Strasser, G. A., Kaminker, J. S. and Tessier-Lavigne, M. (2010). Microarray analysis of retinal endothelial tip cells identifies CXCR4 as a mediator of tip cell morphology and branching. *Blood* **115**, 5102-5110.
Strilic, B., Kucera, T., Eglinger, J., Hughes, M. R., McNagny, K. M., Tsukita, S., Dejana, E., Ferrara, N. and Lammert, E. (2009). The molecular basis of vascular lumen formation in the developing mouse aorta. *Dev. Cell* **17**, 505-515.
Strilic, B., Eglinger, J., Krieg, M., Zeeb, M., Axnick, J., Babal, P., Muller, D. J. and Lammert, E. (2010). Electrostatic cell-surface repulsion initiates lumen formation in developing blood vessels. *Curr. Biol.* **20**, 2003-2009.
Torres-Vazquez, J., Gitler, A. D., Fraser, S. D., Berk, J. D., Van, N. P. J. D., Fishman, M. C., Childs, S., Epstein, J. A. and Weinstein, B. M. (2004). Semaphorin-plexin signaling guides patterning of the developing vasculature. *Dev. Cell* **7**, 117-123.
Wacker, A. and Gerhardt, H. (2011). Endothelial development taking shape. *Curr. Opin. Cell Biol.* **23**, 676-685.
Wang, Y., Kaiser, M. S., Larson, J. D., Nasevicius, A., Clark, K. J., Wadman, S. A., Roberg-Perez, S. E., Ekker, S. C., Hackett, P. B., McGrail, M. et al. (2010). Moesin1 and Ve-cadherin are required in endothelial cells during in vivo tubulogenesis. *Development* **137**, 3119-3128.
Wang, Y., Rovira, M., Yusuff, S. and Parsons, M. J. (2011). Genetic inducible fate mapping in larval zebrafish reveals origins of adult insulin-producing beta-cells. *Development* **138**, 609-617.
Westerfield, M. (2000). *The Zebrafish Book: A Guide for the Laboratory Use of Zebrafish (Danio rerio)*, 4th edn. Eugene: University of Oregon Press.
Zovein, A. C., Luque, A., Turlo, K. A., Hofmann, J. J., Yee, K. M., Becker, M. S., Fassler, R., Mellman, I., Lane, T. F. and Iruela-Arispe, M. L. (2010). Beta1 integrin establishes endothelial cell polarity and arteriolar lumen formation via a Par3-dependent mechanism. *Dev. Cell* **18**, 39-51.

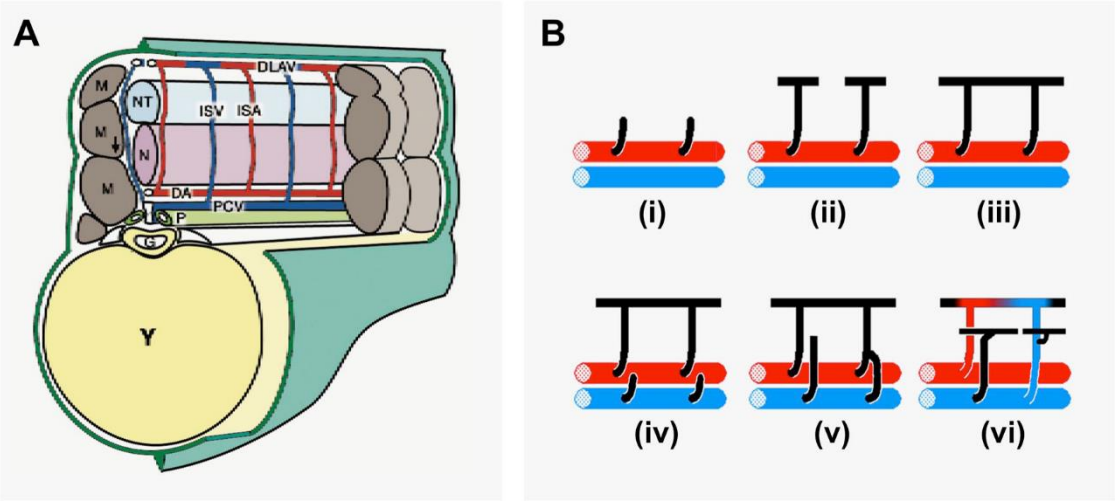

Supplementary Figure 1.

(A) Schematic diagram showing the anatomy of the zebrafish trunk and its blood vessels at approximately 2 days post-fertilization. At this stage there is active flow through the dorsal aorta, (DA), posterior cardinal vein (PCV), and most intersegmental arteries (ISA) and intersegmental veins (ISV). The ISA and ISV are linked together dorsally via paired dorsal longitudinal anastomotic vessels (DLAV). All of these vessels are shown relative to adjacent tissues and structures in the mid-trunk including the gut (G), myotomes (M), notochord (N), neural tube (NT), left pronephric duct (P), and yolk mass (Y). Anterior is to the left and above the plane of the page, and dorsal is up. **(B)** Schematic diagrams illustrating steps leading to assembly of the trunk angiogenic vascular network. For clarity, both diagrams show the vessels on only one side of the trunk. (B.i) Primary sprouts emerge bilaterally exclusively from the dorsal aorta (red). (B.ii) Primary sprouts grow dorsally, branching cranially and caudally at the level of the dorsal-lateral roof of the neural tube. (B.iii) Branches interconnect on either side of the trunk to form two dorsal longitudinal anastomitic vessels (DLAV). (B.iv) Secondary sprouts begin to emerge, exclusively from the posterior cardinal vein (blue). (B.v) Some secondary sprouts connect to the base of primary segments, while others do not. (B.vi) Primary segments with patent connections to secondary segments become intersegmental veins (blue), while primary segments that remain connected only to the dorsal aorta become intersegmental arteries (red). Most of the secondary sprouts that do not connect to primary segments serve instead as ventral roots for the parachordal line (lymphatic progenitors). Intersegmental veins form additional connections to the parachordal vessels at the level of the horizontal myoseptum (arrow). Diagrams are from Isogai et al., Development 130, 5281-5290 (2003).

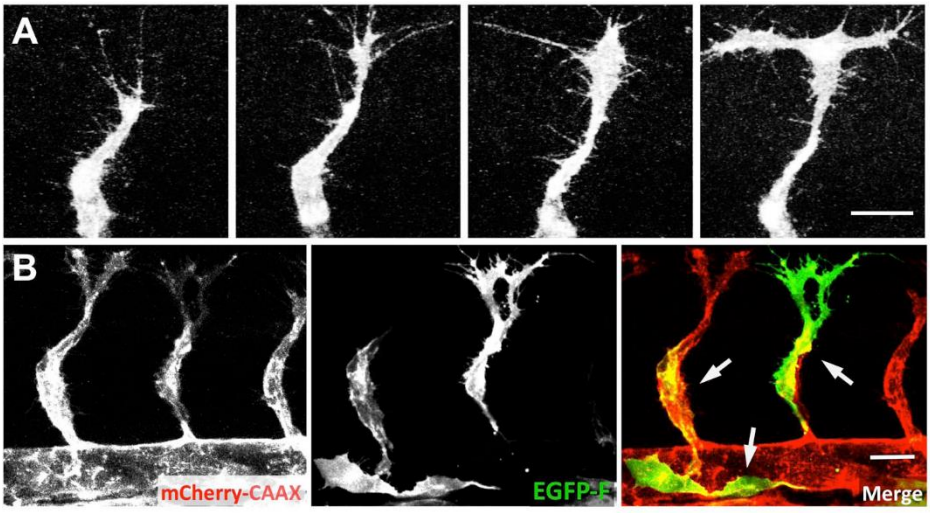

Supplementary Figure 2.

(A) Confocal image time series of a single growing trunk ISV sprout in a *Tg(fli1a:EGFP)*^{y1} embryo, showing dynamic changes in sprout morphology over time**.** **(B)** Confocal image of growing trunk ISV in a 28 hpf *Tg(kdrl:mCherry-caax)*^{y171} embryo injected with a *Tol2(fli1a:EGFP-F)*^{y288} transgene. The injected transgene mosaically marks subsets of endothelial cells, but it is not possible to determine whether contiguously labeled endothelium represents one cell or multiple adjacent cells. All images are lateral views with rostral to the left. Scale bars = 20 µm.

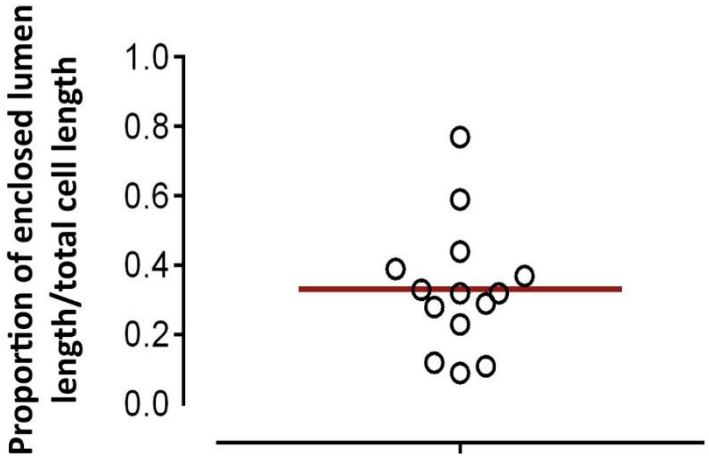

Supplementary Figure 3.

Quantitation of the proportion of each lumen-enclosing single endothelial cell that completely encircles the lumen of trunk ISV or DLAV vessel segments, as a percentage of the total length of the cell along the vessel segment. Each circle represents a single cell. The red line shows the mean value of the percentage of each cell completely encircling the lumen (33%) for all cells counted.

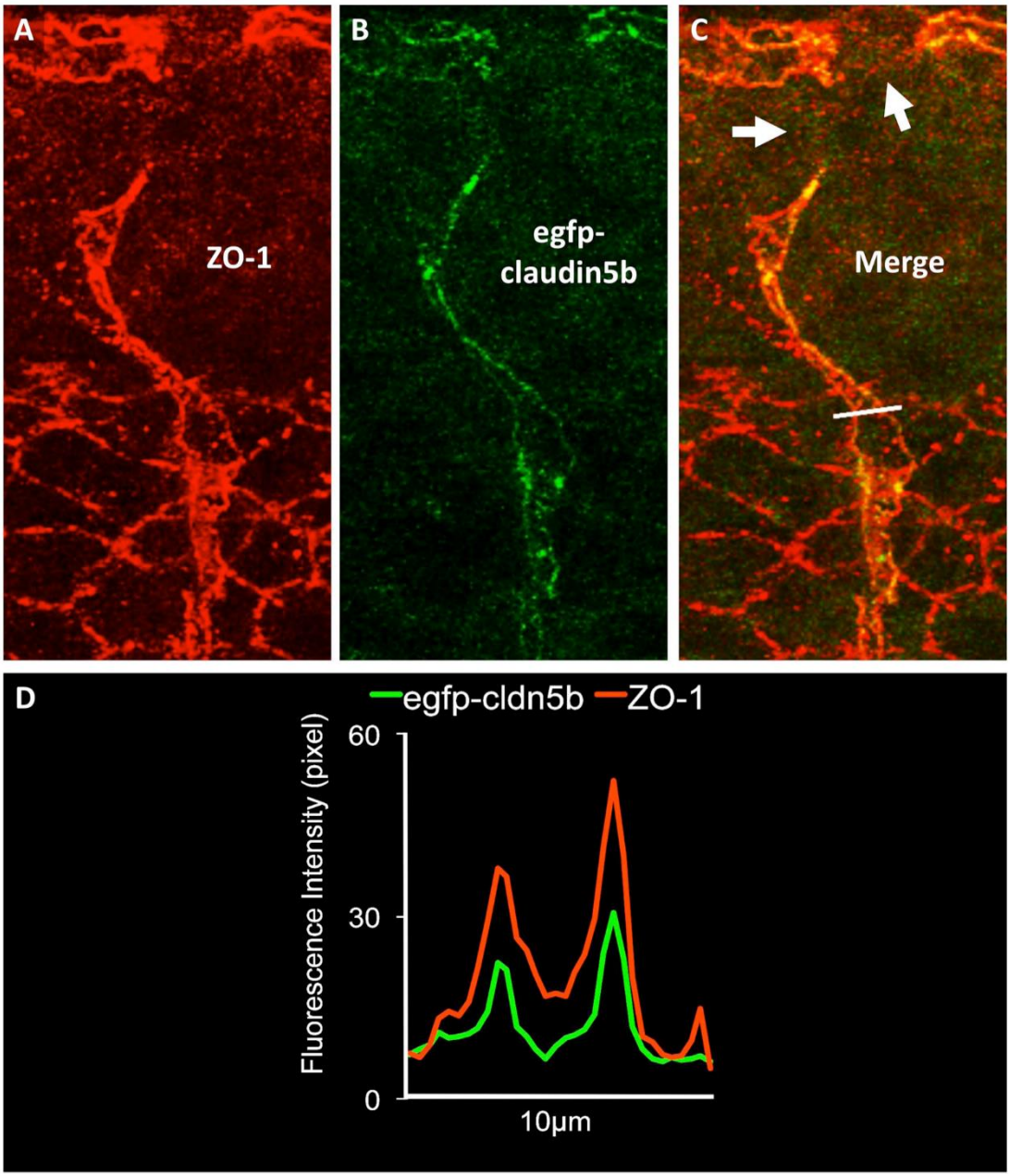

Supplementary Figure 4.

(A-C) Confocal micrograph of whole mount immunohistochemistry of a dorsal trunk ISV/DLAV segment in a 48 hpf *Tg(fli1a:egfp-claudin5b)*^{y287} transgenic animal probed with anti-ZO-1 (panels A,C) and anti-EGFP (panels B,C) antibodies. The white line in panel C shows the trace used to measure red (ZO-1) and green (egfp-claudin5b) fluorescence intensity in panel D. **(D)** Fluorescent pixel intensity of egfp-claudin5b (green) and ZO-1 (red) along the line shown in panel C. Scale bar = 10 µm.

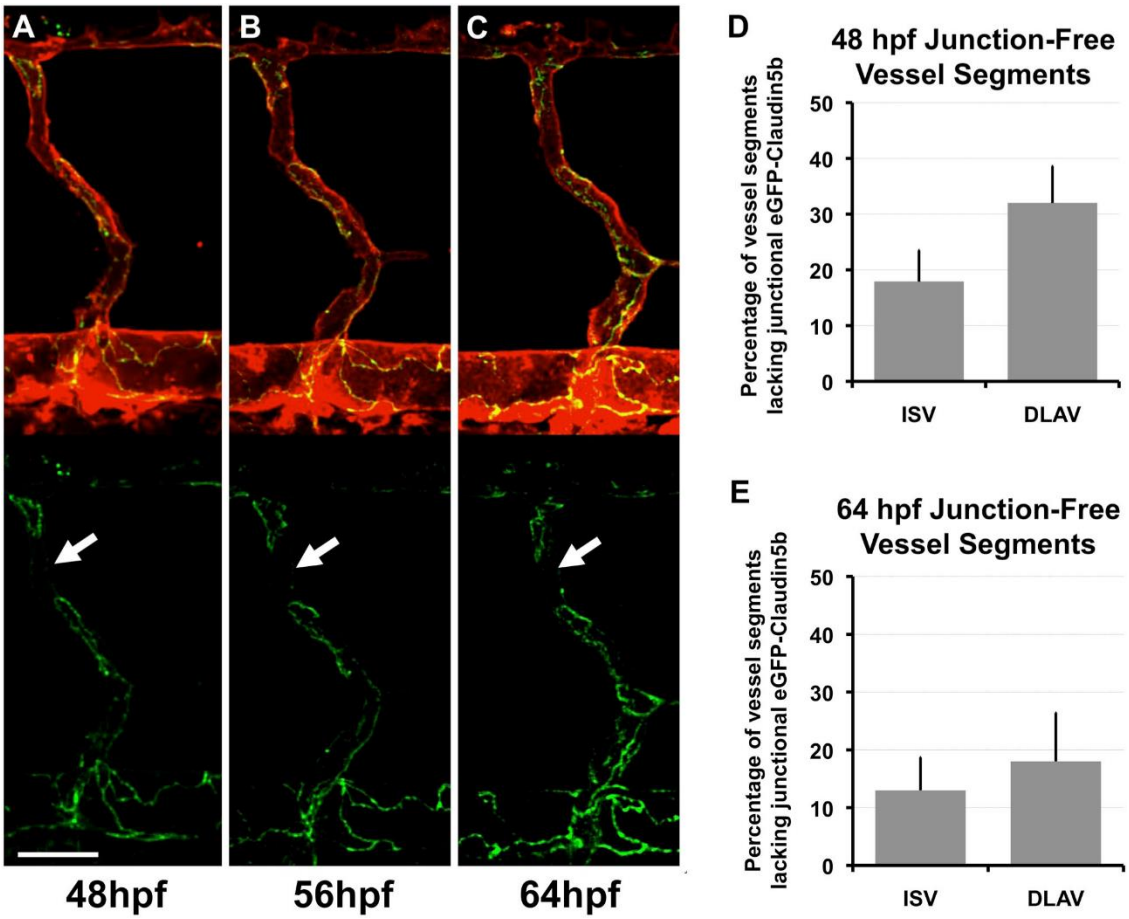

Supplementary Figure 5.

(A-C) Confocal micrographs of mRFP/EGFP (top; EC membranes in red and junctions in green) and EGFP (bottom; junctions in green) fluorescence in the same vascular segments in a *Tg(fli1a:egfp-claudin5b)*^{y287}; *Tg(kdrl:mRFP-F)*^{y286} double transgenic animal at 48 hpf (A), 56 hpf (B), and 64 hpf (C). Tight junction-free vessel segments (arrows) persist for at least a day after intersegmental vessel lumenization**.** **(D,E)** Quantification of the percentage of vessel segments lacking junctional EGFP-Claudin5b, measured in the same *Tg(fli1a:egfp-claudin5b)*^{y287}; *Tg(kdrl:mRFP-F)*^{y286} double transgenic animals at 48hpf (D) and 64 hpf (E). Although junction-free segments persist, the overall length of these segments does decrease over time. Scale bar = 20 µm.

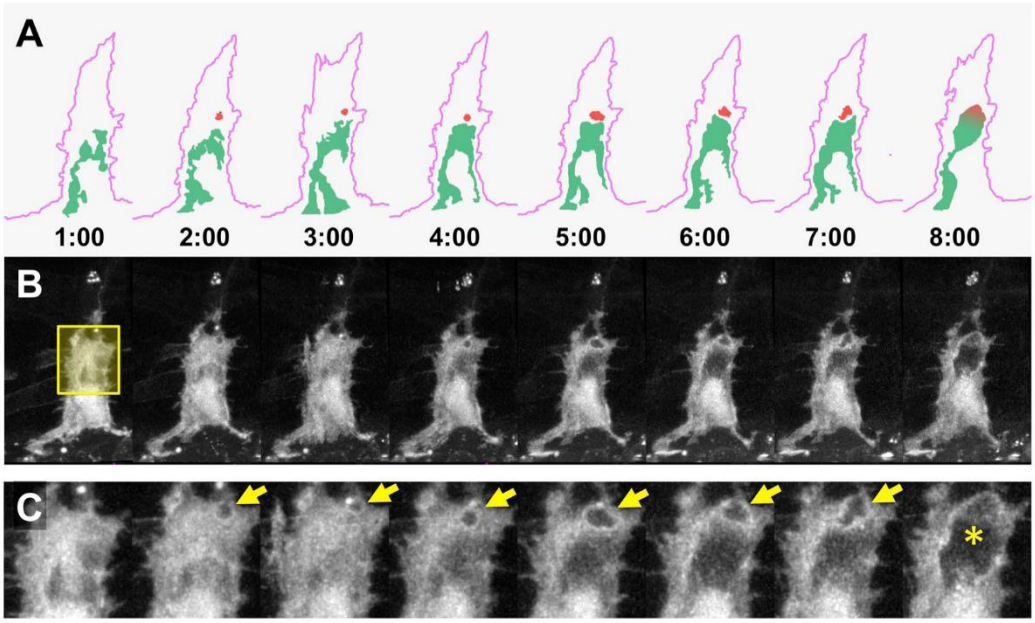

Supplementary Figure 6.

(A) Schematic diagrams illustrating the emergence and enlargement of an intracellular vacuole (red), and its eventual fusion with an extracellular nascent lumen (green) within an intersegmental vessel sprout (outlines in lavender). Elapsed time in minutes is noted. Diagrams correspond to the images below in panels (B) and (C). **(B)** Time series of green fluorescence confocal images (shown in grayscale) of an identified single *(fli1a:H2B-TagBFP-p2A-eGFP-F)* marked endothelial cell in a *Tg(kdrl:mcherry-caax)*^{y171} transgenic animal, showing emergence and enlargement of a vacuole and its eventual fusion with an an extracellular nascent lumen. The yellow box overlaid on the first timepoint image shows the region magnified in panel (C). **(C)** Higher magnification green fluorescence confocal close-up views (shown in grayscale) of the timeseries shown in panel B. Arrows note the position of the newly formed vacuole, while the asterisk marks the compartment into which the vacuole merges in the final image frome. See Supp. Movie 9 for an animation of the time series in panels B and C.

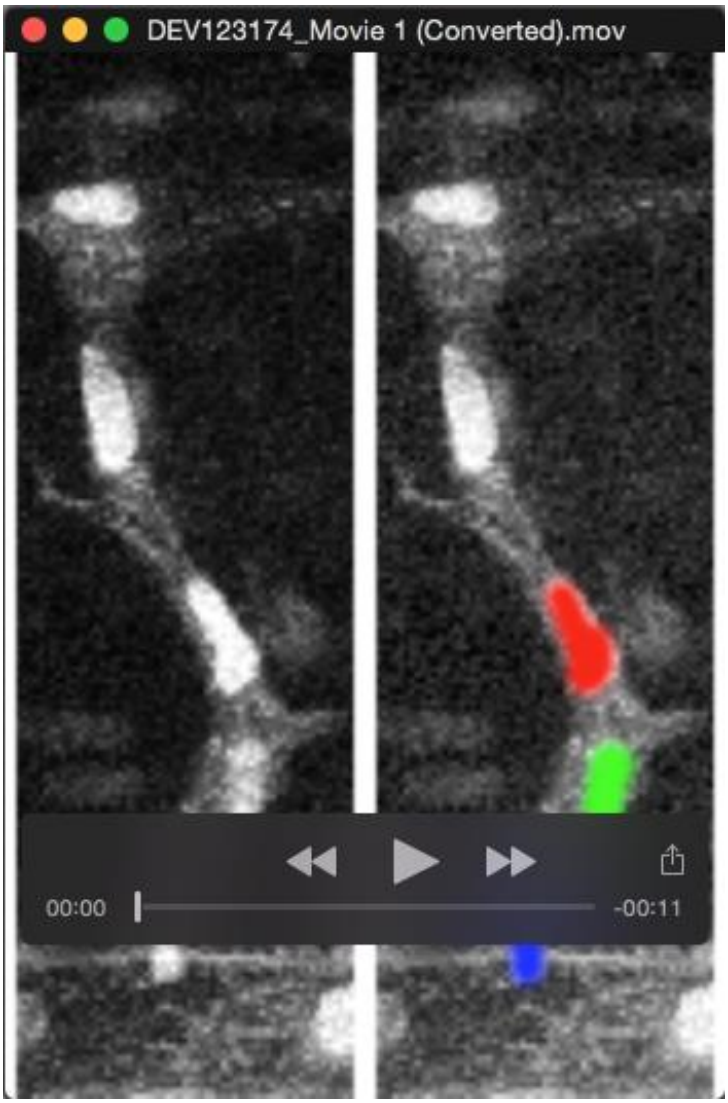

Movie 1.

Time lapse movie of reconstructed confocal images of the nuclear dynamics in *Tg(fli1a:nls-egfp)*^{y7}*; Tg(kdrl:mcherry-caax)*^{y171} double transgenic animals with green fluorescent endothelial cell nuclei and red fluorescent endothelial cell membranes. Selected frames from this movie are shown in Fig. 1C and the positions of the nuclei (in distance from the DA measured along each intersegmental vessel segment) for all frames of the movie are plotted in Fig. 1D. Images were collected every 10 minutes. The movie is shown at a rate of 3 frames/second (30 minutes actual elapsed time per second).

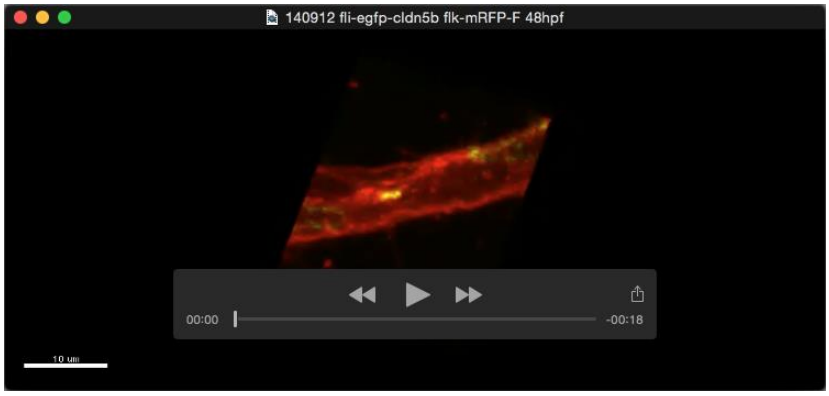

Movie 2.

3-D rotation of a segment of mid-trunk intersegmental vessel in a 30 hpf *Tg(fli1a:egfp-claudin5b)*^{y287}; *Tg(kdrl:mRFP-F)*^{y286} double-transgenic embryo with a "gap" in egfp-claudin5b expression. A corresponding single image if this ISV segment is shown in Fig. 6E.

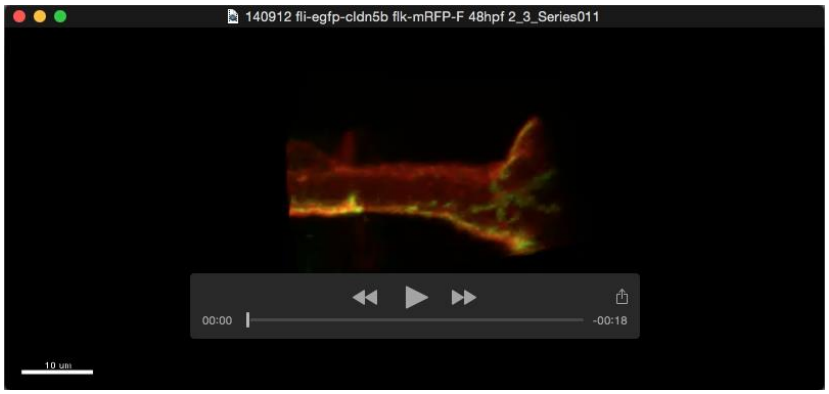

Movie 3.

3-D rotation of a segment of mid-trunk intersegmental vessel in a 30 hpf *Tg(fli1a:egfp-claudin5b)* ^{y287}; *Tg(kdrl:mRFP-F)*^{y286} double-transgenic embryo with a single line of egfp-claudin5b expression. A corresponding single image of this ISV segment is shown in Fig. 6F.

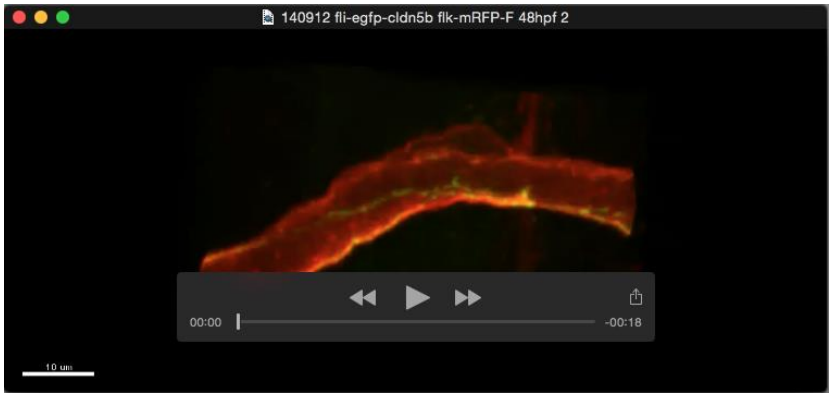

Movie 4.

3-D rotation of a segment of mid-trunk intersegmental vessel in a 30 hpf *Tg(fli1a:egfp-claudin5b)*^{y287}; *Tg(kdrl:mRFP-F)*^{y286} double-transgenic embryo with multiple lines of egfp-claudin5b expression. A corresponding single image of this ISV segment is shown in Fig. 6G.

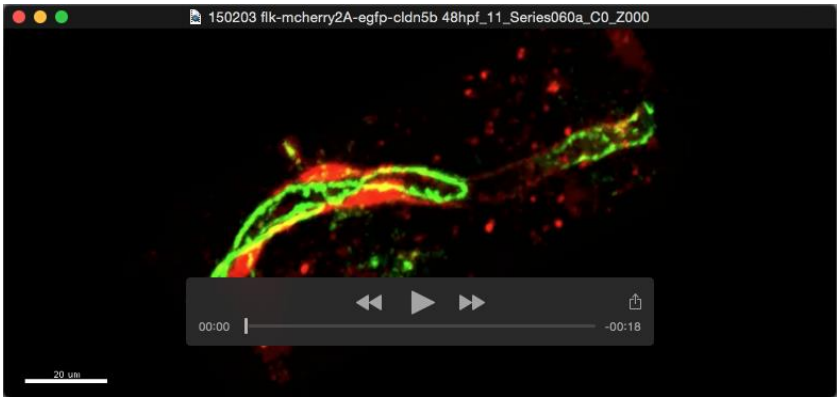

Movie 5.

3-D rotation of reconstructed confocal micrograph stack of a mid-trunk intersegmental vessel in a 30 hpf embryo mosaically expressing an injected *Tol2(kdrl:mCherry-p2A-egfp-claudin5b)* transgene showing merged mCherry/egfp-claudin5b fluorescence. A corresponding single image of this ISV segment is shown in Fig. 6M.

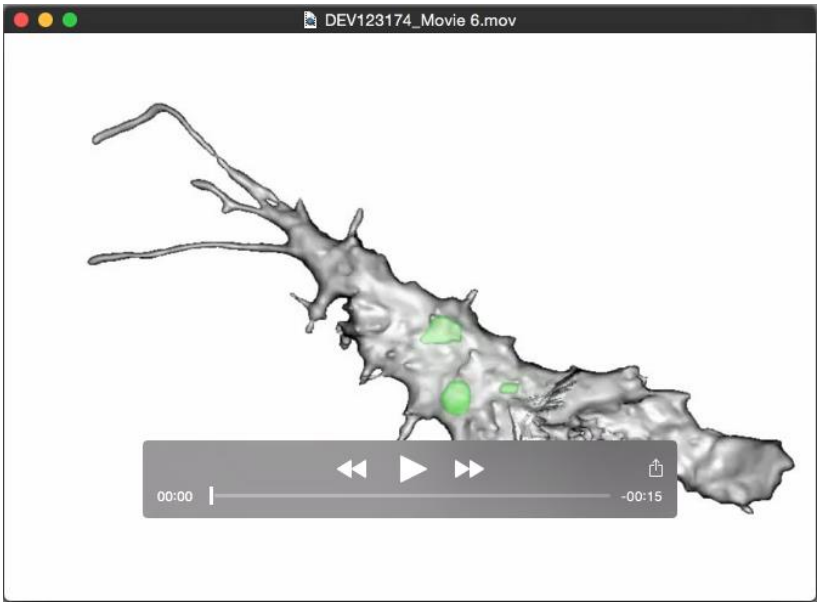

Movie 6.

Image rotation of a surface-rendered 3-D reconstruction of the single endothelial cell shown in Fig. 7A,B. The cell surface is rendered in semi-transparent grey, and internal vesicular/vacuolar structures are rendered in semi-opaque green.

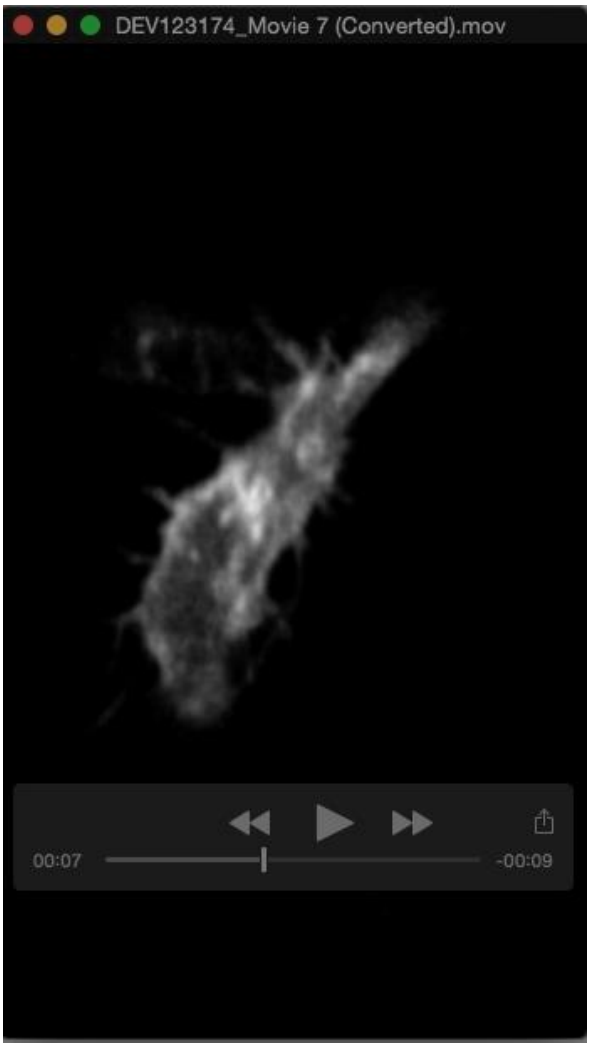

Movie 7.

Deconvolved image stack of a single endothelial cell used to generate the reconstructed images shown in Fig. 7A,B. Spacing between planes is 0.25 µm.

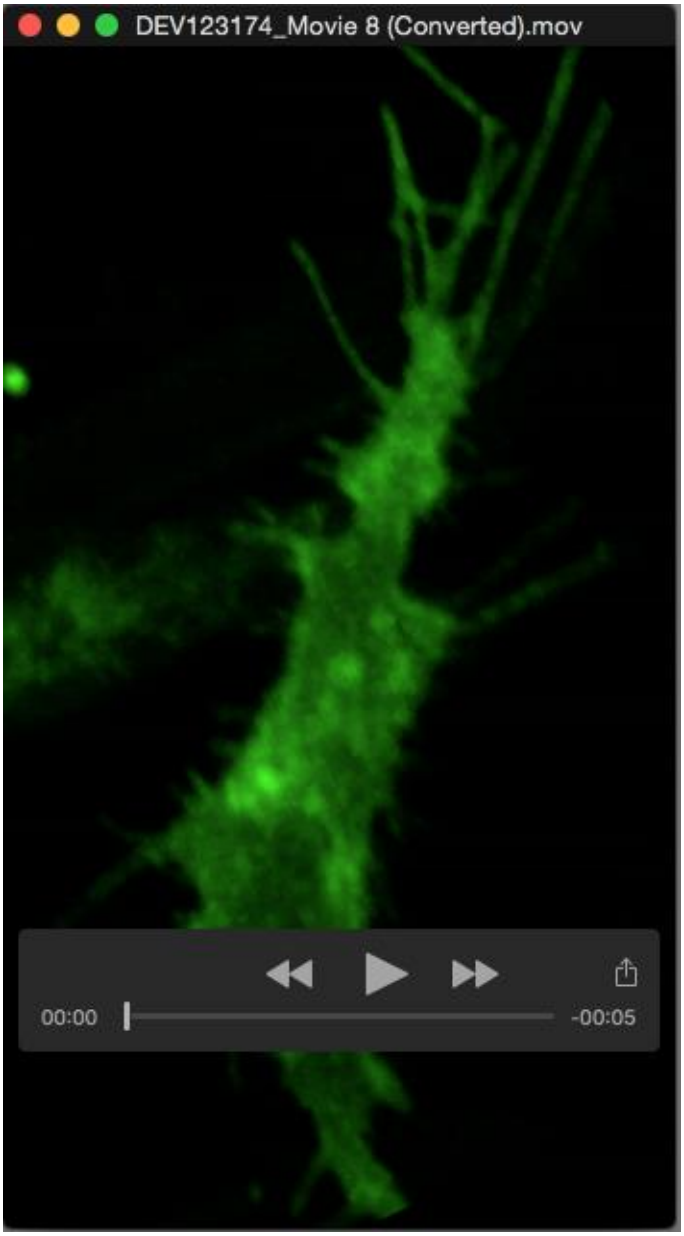

Movie 8.

Time lapse movie of reconstructed confocal images of the single endothelial cell *(fli1a:H2B-TagBFP-p2A-eGFP-F)* morphological changes as shown in Fig. 7C-E. Images were collected every one minute.

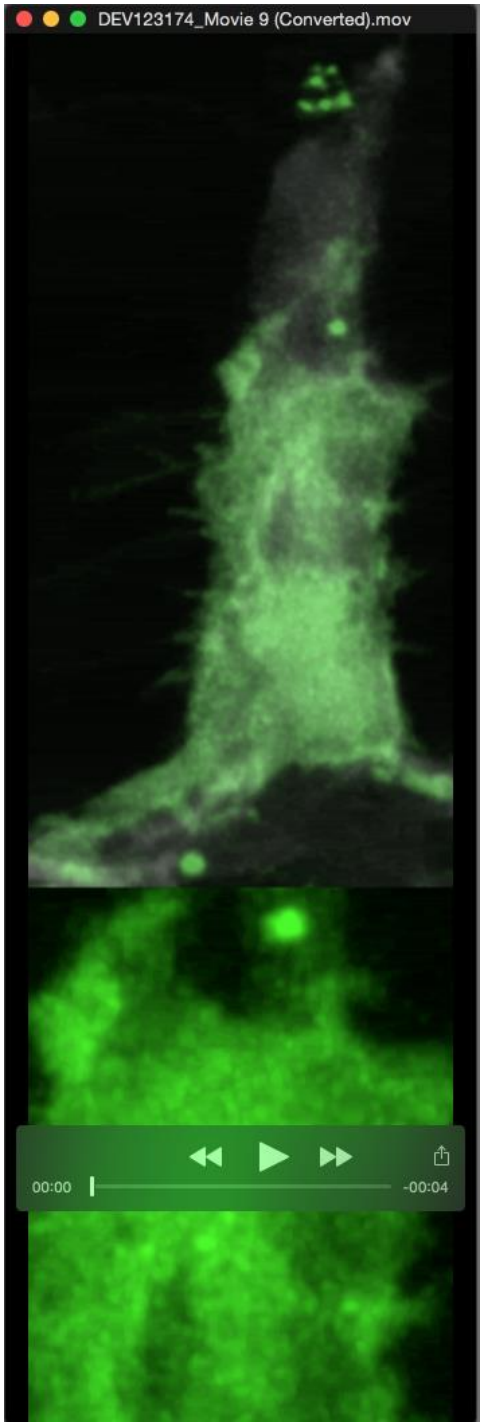

Movie 9.

Time lapse movie of reconstructed confocal images of the single *(fli1a:H2B-TagBFP-p2A-eGFP-F)* marked endothelial cell morphological changes as shown in Supp. Fig. 6. Images were collected once every minute. Top, lower magnification with emerging vacuolar compartment highlighted in red (merging with an extracellular nascent lumen in the final frame). Bottom, corresponding higher magnification views of the vacuole and adjacent nascent lumen.